

Fractal dimension: Problems and traps of its estimation.

Carlos Sevcik MD, PhD, Em. Prof.
Center Biophysics and Biochemistry, (IVIC), Caracas, Venezuela.*

Abstract

This chapter deals with error and uncertainty in data. Treats their measuring methods and meaning. It shows that uncertainty is a natural property of many data sets. Uncertainty is fundamental for the survival of living species, Uncertainty of the “chaos” type occurs in many systems, is fundamental to understand these systems.

Keywords: Fractals, waveforms, rational, numbers, transcendental number

1. Introduction.

1.1. Complexity as a fundamental problem of science.

Complexity is a fundamental characteristic of Our (The?) Universe. Without *complexity* life will not exist [?].

Defining *complexity* is one of the most challenging problems in science [104], some scientists even consider it the most important problem in science [105], *a problem which hinders all modern science*. Complexity is related to entropy, but is a condition between zero entropy and maximum (infinite?) entropy. The problem was first expressed by Maxwell as a “daemon”, [119] and remained unsolved until [203] associated complexity and information. Szilard’s approach leads to the definition of information as *negentropy* [188, 189] and *algorithmic information* [43, 44, 45]. Fractal dimension (D) is also a measure of complexity.

*Current Address: Av. Paralelo 124, Ent 2A, Barcelona, PO Code 08015, Spain. 📞: +34 69766 84n02. ✉: carlos.sevcik.s@gmail.com. ORCID Number: 0000-0003-3783-6541.

1.2. Complexity, uncertainty and experimental error.

The unpredictable data component of a random process studied under constant conditions, may also be called noise. The noise definition is particularly important when a random data sequence is studied, the so called time series. Alterations of conditions where the random may naturally occur, but it may also stem from error when recording data due to instrument failures or due to experimenters mistakes, this is the case of real error.

A common view is to consider data dispersion as ‘errors’, something related with experimenters or equipment ‘mistakes’, which certainly do occur sometimes. Yet, an extremely important source of data uncertainty, is not ‘error’, but a property of the system under study. Such is the case of quantum physics [96] and related disciplines. But fuzziness of data is fundamental importance in biology, if all elements of any population are equal, they can be exterminated by noxae such as a pandemic, or by defects resulting from inbreeding in a small uniform population. When a species is reduced to small sets of individuals, the species is condemned to extinction. Many fundamental biological signals (heart beat, brain signals) in healthy individuals are fuzzy and chaotic, and become less chaotic in pathological states like heart beat [101, 102, 147] or electroencephalographic (EEG) signals [187, 198, 117, 39, 218, 130, 199, 92, 50, 174, 89] (a non exhaustive list of examples). Fractal dimension is also used to analyze lung sounds [74, 73, 90]. Besides biomedical uncertainty, there is a large number of papers using fractal dimension in subjects such as geomagnetic field studies [78], mammary [164], ultrasound studies [46] and machines and materials failures [84, 210] and other situations [60, 190, 179]. Despite the abundance of publications where fractal dimension is calculated, the authors often do not try to understand the mathematics.

In this review we will consider several proposed modes to calculate the fractal dimension [98, 99, 116, 184, 185], and to present several examples of ‘dispersion’ related to chaotic nonlinear systems which are some sources of fractality. We will also consider the Hurst’s coefficient [107] for which a simple relationship with D was proposed [139, 94], a relation currently considered wrong [143, 70, 71, 200].

1.3. Relevance of chaos and dynamical systems.

Complex systems are often called nonlinear systems, strongly sensitive to initial conditions, systems that are also known as ‘dynamical systems’. In these SYSTEMS, there is no randomness, but they change as a result of the

accuracy of the calculations or due to very small environmental variations., The classical example is earth climate shown by Lorenz [133, 132] to be unpredictable, sometimes even at short lapses of time [131, 62, 32].

Lorenz [133, 161], proved that very small changes can produce very large whether changes, ‘the flutter of a butterfly in China can produce a storm in America’, the so-called *butterfly effect*, poetic name that is reinforced by the shape of the Lorenz attractor [133] (See Figure ??). Dynamical systems are totally deterministic, not random, but they are unpredictable [133, 38, 131, 112].

Another form of uncertainty is called chaos. It is central to all fields of human knowledge including quantum physics [26, 225, 103]. This chapter is an introduction to chaos and its difference from the statistical uncertainty to which the rest of this book relates. It is not a new concept started with Lorenz almost 60 years ago [133] and remains central in almost all areas of scientific knowledge.

The impact of Loren butterfly effect on wheather prediction, has determined that the concept of chaos is usually said that was created by Lorenz [133], still the concept is earlier, it was introduced by Turing [209] to explain the source of biological structure and complexity in biology, and by Belousov [24, 106, 224].

Another result of chaos in nonlinear systems is turbulence [163, 115]. A thin layer of ice on an airplaneLorenz’s wings can cause enough turbulence to prevent it from flying. Chaos exists in vital functions such as the normal heart rate which is, within certain limits, chaotic, the absence of chaos in the heart rate indicates disease [165, 75, 111, 168, 166, 101, 167], but if the chaoticity becomes extreme (the so-called ventricular fibrillation) it causes death. Examples of the significance of chaos are too many to cite here, this includes earthquakes [53], fluctuations in the stock market and the economy in general [135, 135, 142, 125], a couple of somewhat classic references are [139, 94].

1.4. Lorenz’s Uncertainty.

But uncertainty is not just “error”. his was first shown in a log neglected model of wheather studied by Lorenz [133] (S the system of Eqs. (1)). Lorenz’s system of equations was certainly sensitive to rounding errors, and the limited accuracy of the analog computer available to him. But the strange set of solutions (resembling a butterfly), although constrained

to a definite volume of an Euclidean space, never crossed it self at a previous point (solution). The system was also unpredictable, it changed if was initialized with apparently similar values.

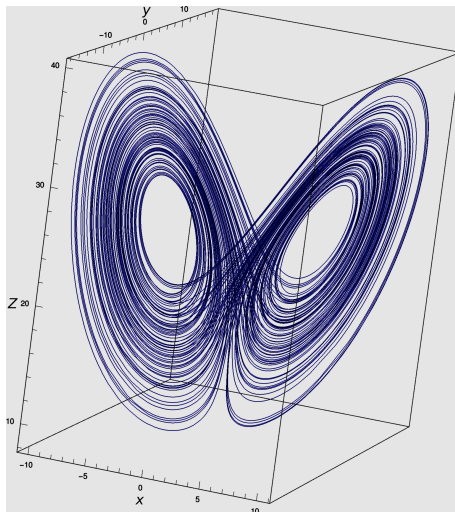


Figure 1: **Lorenz's attractor [133]**. Latin letters x, y, z represent an Euclidean three dimensional system coordinates. Example's constant values are: $\sigma = 3; \rho = 26.5; \beta = 1$; initial coordinate's values are $x_0 = -1; y_0 = 0; z_0 = 1$. Figure presents 40000 consecutive solutions of the system of equations solutions (1).

All possible values in a dynamic system usually exist in a finite space and are distributed in a region of that space called attractor. A classical example is Lorenz's attractor [133], shown in Figure ?? and represents the solutions of a simple set of differential equation built by Lorenz as a atmospheric climate model. Lorenz's equations are [133, 161, 132]:

$$\frac{dx}{dt} = \sigma(y - x) \quad \frac{dy}{dt} = \rho x - xz - y \quad \frac{dz}{dt} = xy - \beta z \quad (1)$$

where x, y and z are the coordinates of an Euclidean system. Figure ?? represents a series of solutions of this system. The trace in the figure represents a single continuous, which never crosses through the same, previous, point, and repeats unpredictable displacements of which are solutions of the equation's system. Perhaps the most important properties of the graphic, is that all solutions are confined in a subset (volume) of the Euclidean space called a strange attractor, Equation system (1) was built by Lorenz as a climate model, is the first es el primer *strange attractor* known and to describe

climate (we also call it whether) and it showed that real whether (much more complex than the model) is unpredictable (except for short periods), changing the history of meteorology. Having a strange attractor is not unique to Lorenz's system, many other systems have strange attractors too.

Climate unpredictability has been well demonstrated after Lorenz. Whether can only be predicted for short periods even with modern supercomputers of today, receiving information from sensors spread all over the world. Lorenz's equations in laser models [91], electricity dynamos [118], convection loops [77], direct current motors without brushes [97], electric circuits [51] and chemical reactions [170] among many more systems. Lorenz's-like systems are not this book's object of study but they must be considered by its reader, since *statistical methods are often applied to Lorenz-like dynamic systems, and are used to predict the properties of such systems, and the predictions failure is wrongly attributed to statistics and not to their unpredictable nature*. An example of this opinion studies, which when are made public, may (usually do) modify the public opinion that they *objectively* claim to study. In politics, it sometimes results it is common 'to bet on the winner' voting for or against him or her if a candidate produces fear. Classical examples of this effect is also the expectation produced by a medical treatment (which may lead to changing or selecting the proved that study subject or the experimenters performing the study), they could even modify the results observed (i.e. change the result). increasing the beneficial or adverse effects of the treatment studied, having or not having faith in the treatment could be another example. This is an extension of the quantum physics observer effect, extended to daily supra molecular. Lorenzian uncertainty was later called *chaos*, and was the first system known to contain *chaotic* uncertainty.

2. Time Series and the Fractal Dimension.

2.1. The concept of fractality.

We define here as time series what, perhaps in better but longer common English, should be called: *series of events which occur in time*. A set presented as a graph where the ordinate represents random events and the abscissa is the time at which each event occurs.

Studying systems, living or not, as dynamical (chaotic, as they are commonly called) nonlinear systems is of great interest in biology and medicine [65]. Fractal dimension analysis is a possible way to characterize dynamical systems and other complex curves and time series analysis is one of the most

common ways used to calculate the fractal dimension from observables [65]. Time series analysis is also interesting *per se*. However, this analysis can be related to complex concepts such as regularity, complexity or spatial extension [139, 157, 168]. A good example can be found in two series constructed by Pincus *et al.* [168] to illustrate the complexities of heartbeat in healthy and diseased humans, these are:

90, 70, 90, 70, 90, 70, 90, 70, 90, 70, 90, 70, 90, 70, 90, 70, . . .

and

90, 70, 70, 90, 90, 90, 70, 70, 90, 90, 70, 90, 70, 70, 90, 70, . . .

The two series have the same mean and the same variance and the two values (90 or 70) have the same probability of occurring: $\frac{1}{2}$. Rank statistics also do not distinguish between them. However, the two series are completely different; In the first we always know with total certainty which number follows once we observe an element of the series. In the second series, we only know that it will be 90 or 70, but our choice will be false in 50% of cases.

The English term *waveform*, which we translate here as “waveform” refers to the appearance of a wave much more complex than a “ripple” as defined by the Meriam Webster’s Dictionary, usually periodic *versus* time. Any waveform is a series of points. Apart from classical statistical models such as statistical moments [87] and regression analysis, properties such as Kolmogorov-Sinai entropy [81], the apparent entropy [168] and the fractal dimension [116] have been proposed to address the problem of analyzing waveforms. The fractal dimension can provide information about spatial extension (tortuosity or its ability to fill space) and its self-similarity (ability to remain unchanged when the measurement scale changes), its self-affinity [20]. Unfortunately, although there are rigorous methods for calculating the fractal dimension [82, 83, 16?], their usefulness is severely limited since they demand great computing power and because their evaluation is time-consuming. In Euclidean space, waveforms are flat, two-dimensional curves.

“Clouds are not spheres, mountains are not cones, coastlines are not circles, and bark is not smooth, nor lightning travel in a straight line. [139]”

Fractal geometry was introduced by Mandelbrot to describe natural forms.

“fractal from the Latin adjective *fractus*. The corresponding Latin verb *frangere* "to break:" to create irregular fragments. . . . *fractus* should also mean “irregular” [139]”

Nature is, above all is, *complex*,

“Nature exhibits not simply a higher degree but an altogether different level of complexity[139].”

According to Mandelbrot [139, pg. 15 and Chap. 39]:

“A fractal is by definition a set for which the Hausdorff-Besicovitch dimension strictly exceeds the topological dimension. Every set with a non integer D is a fractal.”

2.2. The Hausdorff–Besicovitch dimension.

The Hausdorff–Besicovitch dimension (D_{HB}) [95, 27] of a metric space (for which a metric dimension can be defined) of a set can be defined as [139]:

$$D_{HB} = -\lim_{\epsilon \rightarrow 0} \frac{\ln[N(\epsilon)]}{\ln(\epsilon)} = -\lim_{\epsilon \rightarrow 0} \log_{\epsilon}[N(\epsilon)] \quad (2)$$

where $N(\epsilon)$ is the number of open balls of radius ϵ needed to cover the set. In a metric space, given any point X , an open ball with sceptor in X and radius ϵ , is a set of all points x for which the distance between the points X and x is less than ϵ , that is: $dist [|x - X|]$.

The term waveform applies to the form of a wave usually drawn as a value at an instant, of a periodic nature, versus time. A classic example is momentum statistics and regression analysis, properties such as the Kolmodorov-Sinai entropy [81], the apparent entropy [168] and the fractal dimension [184, 185] have been proposed to perform waveform regression analysis. the fractal dimension can provide information on statistical extent (tortuosity or the ability to fill space) and similarity (the ability to remain unchanged when the measurement scale changes) and self-affinity [20]. In processes occurring in two Euclidean dimensions, waveforms are curves with coordinates, x and y , which *usually have different units*.

2.3. Waveforms with non integer D_{HB} .

For a number of waveforms

$$(D_{HB} \in \mathbb{R}) \wedge (D_{HB} \notin \mathbb{C})$$

where \mathbb{R} is the set of real numbers, and \mathbb{C} is the set of all complex numbers. which does not necessarily mean that $D_{HB} > 1$. There are also functions such as, for example, the call ‘dust’ or Cantor set [40, 175, 55, 7, 9] for which $D_{HB} = \frac{\log(2)}{\log(3)} = 0.630929753571\dots$. These waveforms correspond to infinite disjoint sets of points which, however, constitute a waveform [9].

In an Euclidean system on $n_E \in \mathbb{Z}$ dimensions¹

$$D_{HB} \in \{0 \leftrightarrow n_E\} \in \mathbb{R} \quad (3)$$

which implies $\{0 < D_{HB} \leq 1\}$. In words, $D_h B$, or in general D are real positive numbers, which may be smaller than 1. This occurs in Cantor sets [40, 7] also called “Cantor dust” in one dimensional Euclidean spaces.

3. Estimators of fractal dimension.

3.1. The dimension of a waveform suggested by Katz [116].

Fractal waveform analysis was initially proposed by Katz [116], who proposed that the complexity of a waveform can be represented by what Mandelbrot [139] called the fractal dimension, and represented by Katz as Φ (represented as D_K in this book). Katz [116] said that the fractal dimension taking N samples measured empirically at constant intervals of the abscissa of the waveform.

Katz’s equation [116] was based on an observation by Mandelbrot [139] where he pointed out that river courses were fractal structures where the fractal dimension could be approximated with an equation similar to Katz’s, relating the length of the riverbed, with the greater distance separating two points of the river basin.

The procedure suggested by Katz [116] discretizes the waveform producing $N' = N - 1$ rectilinear segments from which with the notation, with the equation of Katz’s [116] below:

$$\Phi = \frac{\log(N')}{\log(N') + \log(d/L)} = D_K \quad (4)$$

¹ \mathbb{Z} = set of all integers numbers; \leftrightarrow = indicates a set of numbers limiters

where d is the *planar extension* of the [139, Chapter 12] curve and L is the length of the discretized curve defined as:

$$\begin{aligned} d &= \max [\text{dist}(i, j)] \\ L &= \sum_{i=0}^{N'} \text{dist}(i, i + 1) \end{aligned} \quad (5)$$

where \max means the maximum $\text{dist}(i, j)$, of the distance the points i and j of the curve. For a curve that does not cross itself usually, but not always, $d = \max [\text{dist}(1, i)]$.

3.2. *Sevcik's fractal dimension [184, 185]: a simple method to calculate the fractal dimension of waveforms.*

An expression to calculate the fractal dimension of a waveform is obtained from the Hausdorff–Besicovitch (D_{HB}) dimension [95, 27]. Mandelbrot's fractal (see for example [140]) is real number, not an integer. The Hausdorff–Besicovitch dimension [140] of a metric space can be expressed (for a very understandable discussion of metric spaces see Barnsley [20]) as:

$$D_{HB} = -\lim_{\epsilon \rightarrow 0} \frac{\ln[N(\epsilon)]}{\ln(\epsilon)} = \lim_{\epsilon \rightarrow 0} \log_{\epsilon} [N(\epsilon)] \quad (6)$$

where the notation is equal to that of Eq. (2). In a metric space given any point P , an open ball with center at P , ϵ , is the set of all points x for which $\text{dist}(P, x) < \epsilon$, at any length L can be divided into $N(\epsilon) = L/(2 \cdot \epsilon)$ long segments $2 \cdot \epsilon$, and any of them be covered by N open balls of radius ϵ . Therefore Eq. (6) can be rewritten as

$$\begin{aligned} D_{HB} &= \lim_{\epsilon \rightarrow 0} \left[\frac{-\ln(L) + \ln(2 \cdot \epsilon)}{\ln(\epsilon)} \right] \\ &\dots = \lim_{\epsilon \rightarrow 0} \left[1 - \frac{\ln(L) - \ln(2)}{\ln(\epsilon)} \right]. \quad (7) \\ \therefore D_{HB} &= \lim_{\epsilon \rightarrow 0} \left[1 - \frac{\ln(L)}{\ln(\epsilon)} \right] \quad \square \end{aligned}$$

Waveforms in two dimensions are sets of points with coordinates which may have distinct units. Since the topology of a metric space does not change under linear transformations, it is convenient to linearly transform

one waveform into another in a normalized space, where all axes are equal and have length 1. This can be done with two linear transformations embedded into an equivalent metric space. The first transformation normalizes the curve's abscissa as:

$$x_i^* = \frac{x_i}{x_{max}}. \quad (8)$$

Where x_i are the original values of the abscissa, and x_{max} is the maximum x_i . The second transform normalizes the ordinate as follows:

$$y_i^* = \frac{y_i - y_{min}}{y_{max} - y_{min}} \quad (9)$$

where y_i are the original values of the ordinate, and y_{min} and y_{max} are the minimum and maximum y_i , respectively.

The two linear transformations map N points of the transform into another that belongs to a unit square. This square can be displayed as a grid of $N \cdot N$ cells. N of them containing a point of the transformed wave. A linear transformation applied to a function in a linear metric space does not alter the Calculating L of the transformed wave and Rolando $\epsilon = 1/(2 \cdot N')$ the Eq. (7) is made

$$\begin{aligned} D_{HB} &= \Phi \\ \dots &= \lim_{N' \rightarrow \infty} \left(1 + \frac{\ln(L)}{\ln(2 \cdot N')} \right) \\ \therefore \mathbf{D}_{HB} &= \Phi = \lim_{N' \rightarrow \infty} (D_S) \quad \square \end{aligned} \quad (10)$$

the approximation to Φ expressed in Eq. (7) expressed in Eq. (10), improves as $N' \rightarrow \infty$. The Eq. (10) as simply D , in [184, 185] as an anonymous derivative of the Hausdorff-Besicovitch dimension [27, 95], this fractal dimension estimator has been called with increasing frequency: "Sevcik's" dimension [190, 54, 191, 155, 221, 121]. So since our work of 2022 [179] we call it "Sevcik's fractal dimension", D_S .

3.2.1. Approximation to the variance of D_S .

Although Φ is a topological invariant of a set and a metric space, D_S is only an empirical estimate of Φ with some uncertainty based on a set of points sampled from a wave; D_S is therefore a random variable. The ratio between Φ and D_S is similar to that between a mean of a *population* (μ)

and the mean \bar{x} estimated when sampling the population; Although μ is a population invariant, \bar{x} will change with sampling. Just as \bar{x} converges towards μ as the sample approaches population size, D_S converges towards Φ as $N' \rightarrow \infty$. Now we will derive an expression for $\text{var}(D_S)$ (the variance of the D_S) from the estimate of D_S obtained by mastering N' points of a wave. It should be obvious from the derivation of D_S and the non-stationary character of the values of D_S determined with Eq. (10), $\text{var}[(D_S)]$ does not provide information about the asymptotic value of D_S obtained as $N' \rightarrow \infty$. The variance of D_S can be estimated starting from the following expression:

$$\begin{aligned} \text{var}[D_S] &= \text{var}\left[1 + \frac{\ln(L)}{\ln(2 \cdot N')}\right] \\ \therefore \text{var}[D_S] &= \text{var}\left[\frac{\ln(L)}{\ln(2 \cdot N')}\right] \quad \square \end{aligned} \quad (11)$$

The approximate solution to Eq. (11) can be obtained by recalling that the variance any random variable set may be $\{x_i\}$ approximated with a Taylor series (see for example [48]) as:

$$\begin{aligned} &\text{var}[x_1, x_2, \dots, x_i, \dots, x_k] \\ \dots \approx &\sum_{i=1}^k \left[\left(\frac{\partial [f(x_1, x_2, \dots, x_i, \dots, x_k)]}{\partial x_i} \right)^2 \cdot \text{var}(x_i) \right] \end{aligned} \quad (12)$$

which for Eq. (12) produces:

$$\text{var}[D_S] = \frac{\text{var}[L]}{L^2 \cdot \ln(2 \cdot N')^2} \quad (13)$$

as L is the sum of N' segments of length Δy , Eq. (13) is equivalent to

$$\text{var}[D_S] = \frac{N' \cdot \text{var}[\Delta(y)]}{L^2 \cdot \ln(2 \cdot N')^2}$$

where $\text{var}(\Delta y)$ may be estimated from the data as:

$$\text{var}[\Delta y] = \frac{1}{N'} \sum_{i=1}^N (\Delta x_i - \overline{\Delta x})^2 \quad (14)$$

where $\overline{\Delta y}$ is the mean length of the segments. In this way combining Eqs. (3.2.1) and (14) we get:

$$\therefore \text{var}[D_S] = \frac{\sum_{i=1}^N (\Delta x_i - \overline{\Delta x})^2}{L^2 \ln(2 \cdot N')^2} \quad \square. \quad (15)$$

3.2.2. *Convergence of D_S towards D_{HB} , an analytic solution for Koch's triadic curve.*

The asymptotic convergence of D_S to Φ can be proven from the Koch triad. Although I derived the equation (10) for waves, that is, plane curves that are sets of pairs of dots (x_i, y_i) such as $x_i \rightarrow \infty$ when $i \rightarrow \infty$. However, on at least some occasions the utility of $D_S \Phi$ extends to the field of waveforms, I will demonstrate that with the famous Koch triad shown in Figure 2.

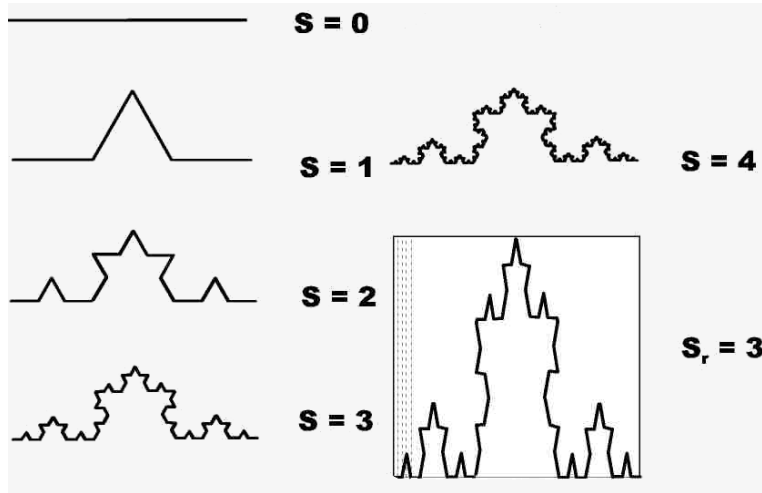


Figure 2: **Characterization of the Koch curve.** The Koch curve is built on the three sides of an equilateral triangle, here I consider a single side to better visualize the convergence $D_S \rightarrow D_{HB}$ for the Koch's snowflake. I start with a line of length 1. Above and to the left of the graph (Stage 0 or $S = 0$, in the figure) a line of length 1 ($\lambda = 1$) is presented. Then, at each stage, a segment of length $\frac{\lambda \cdot S}{3}$ is cut and moved up from each straight line, and an equal segment of length $\frac{\lambda \cdot S}{3}$ is added forming two sides of a new "triangle" lacking its "basal" segment. Repeating this an infinite number of times, one obtains Koch's snowflake, each S stage is indicated by the letter $S = 0, 1, 2, \dots, \infty$. Below and to the right of the figure, stage 3 ($S = 2$) is shown scaled into a square of side 1, in stage 3 ($S_r = 3$), see the text for more details. This figure was adapted from Figure 4 of [184, 185].

The following properties can be easily verified to be true for the triadic

curve at any stage. S :

$$\begin{aligned}
n_s &= 2^{2S} & L &= \left[\frac{4}{3}\right]^S \\
l_s &= 3^{-S} & n_{hs} &= \frac{2^{2S}-1}{3} + 1 \\
n_{is} &= 2^{2S} - \left(\frac{2^{2S}-1}{3} + 1\right) & n_v &= 2^{2S} - 1
\end{aligned} \tag{16}$$

$$K_h = \frac{1}{\sqrt{12}}$$

where: S , is the number of the stage (as used in Figure 2); n_s , is the number of segments that form a curve; L , the length of the curve; l_s , is the length of each segment; n_{hs} , is the number of segments that have ‘‘horizontal’’ segments (that is, they can be extended as a line parallel to the line parallel to segment 0); n_{is} , is the number of ‘‘inclined’’ segments (This is non-horizontal as defined relative to n_{hs} ; n_v is the number vertex on the curve; K_h is the height of the equilateral triangles constructed in stage 1, measured perpendicular to the line extending the horizontal segments at its base. This centers the open ball elements of radius.

$$\epsilon = \frac{3^{-S}}{2}$$

at both terminals of the triadic curve, and at each intersection of segments on the curve, therefore, we have

$$N(\epsilon) = 1 + 2^{2S}$$

of those open balls that are required to cover the curve. starting from the expression for ϵ and $N(\epsilon)$ and Eq. (2) we obtain the fractal dimension (Hausdorff-Besicovitch) of the curve as:

$$D_{HB} = \lim_{S \rightarrow \infty} - \frac{\ln(1 + 2^{2S})}{\ln\left(\frac{3^{-S}}{2}\right)} = \frac{\ln(4)}{\ln(3)} = 1.2618\dots$$

which is also the similarity and coverage dimension of the triadic curve. To test the capability of the Eq. (10) to predict D_{HB} in any case of the triadic curve we have to transform the curve as follows:

$$\begin{aligned}
x_i^* &= x_i \\
y_i^* &= y_i \cdot \sqrt{12}
\end{aligned}$$

This is shown at the bottom of Figure 2 for the 3^S stage of the build process. The transformation does not modify the length of the horizontal components of the Koch curve but extends the length of all inclined sections that it becomes.

$$l_{is} = \sqrt{\frac{1}{6^{2 \cdot S}} + \frac{12}{6^{2 \cdot S}}} = \frac{\sqrt{13}}{6^S}.$$

And the curve at this stage becomes S and we have

$$L = n_{hs} \cdot l_s + n_s \cdot l_{is} = \left(\frac{2^{2 \cdot S} - 1}{3} + 1 \right) \cdot \frac{1}{3^S} + \left[2^{2 \cdot S} - \left(\frac{2^{2 \cdot S} - 1}{3} + 1 \right) \right] \cdot \frac{\sqrt{13}}{6^S}$$

then, in order to provide that each vertex of the curve corresponds to a cell of the normalized square we have that

$$N' = 3^S$$

is outlined as dotted lines in Figure 4 ($s_r = 3$). Replacing in Eq. (10)

$$\begin{aligned} D_S &= \lim_{S \rightarrow \infty} \left[1 + \frac{\ln \left\{ \left(\frac{2^{2 \cdot S} - 1}{3} + 1 \right) \cdot \frac{1}{3^S} + \left[2^{2 \cdot S} - \left(\frac{2^{2 \cdot S} - 1}{3} + 1 \right) \right] \cdot \frac{\sqrt{13}}{6^S} \right\}}{\ln(2 \cdot 3^S)} \right] \\ &\dots = \frac{\ln(4)}{\ln(3)} \\ \therefore D_S &= \frac{\ln(4)}{\ln(3)} = D_{HB} = \Phi = 1.26185950714\dots \quad \square \end{aligned} \tag{17}$$

as it should be. **Thus, the limit of D_S is indeed Φ when $N \rightarrow \infty$ [184, 185].**

3.2.3. Sevcik's fractal dimension convergence to D_{HB} .

The main limitation of D_S is that the speed of convergence towards D_{HB} , the latter is, generally speaking, unknown. Processes such as the one described by Eq. (17) suggest that convergence occurs, but say little about the speed of convergence.

Part of the problem is that the original convergence presumes that in the set of pairs $\{(x_i, \in \mathbb{R}) \wedge (y_i \in \mathbb{R})\}$, but this is not necessarily always true. Then: What happens, if we use expressions (10) and (15) but $\{(x_i, \notin \mathbb{R}) \vee (y_i \notin \mathbb{R})\}$?. This is the case when using D_S to determine whether the

series of digits of π is infinitely aperiodic, which in the field of aperiodic, non-rational numbers also called normal (**without, in this case, having any relation to the Gauss pdf**) [183, 186] :

The question has been asked by many authors [17, 18]. The definition of normal number [30] is [193, pg. 299]: Let g be a natural number > 1 ; we write a real number $x = [x] + (0.c_1c_2c_3\dots)_g$ as a decimal in the scale of g .

For any digit c (on the scale g) and each natural number $n \in \mathbb{N}$, we denote $I(c, n)$ the number of those digits in the sequence c_1, c_2, \dots, c_n , which are equal to c . Then

$$\lim_{n \rightarrow \infty} \left[\frac{I(c, n)}{n} \right] = \frac{1}{g}$$

For each of the 9 values $\neq 0$ of c , then the number x called normal on the scale of g . A number that is normal on the g scale is called absolutely normal [22]. For a number with base 10, the definition implies that $c_i \in \mathbb{N}[0, 9]$ if it must be true for any number $x \in \mathbb{R}$ as $N \rightarrow \infty$. Therefore, various authors use statistical tests such as comparing the frequencies of each digit in the sequences of the decimals of π , and the frequencies of various combinations of decimal digits [19]. This approach is unsatisfactory since all possible combinations cannot be evaluated, and is limited by the N values of other series studied, as well as by the size of sub samples of which N was selected to perform statistical tests.

The fractal analysis described [183, 186] considered the set of decimals of π , and calculated its approximate fractal dimension D_S for $N = 10^1, 10^2, 10^3, \dots, 10^9$ and showed that

$$\lim_{N \rightarrow \infty} D_S \approx 2$$

All series of type $y_i = f(\{\theta_k\}_i)$, where $f(\{\theta_k\}_i)$ is some kind of random variable that depends on a set of parameters. This was found true in [183, 186] for series of **independent** real random numbers distributed with a pdf such as Gauss', Poisson's, exponential, or uniform $U_{\mathbb{R}}[0, 1]$, as well as discrete distributions such as $U_{\mathbb{Z}}[0, 9]$ for the decimal sequence of π . We have also seen that D_S for series by observing the condition represented as the equation²

$$(y_i \perp\!\!\!\perp y_{k \neq i}) \forall y_{k \neq i} \Rightarrow \lim_{N \rightarrow \infty} D_S = 2, \quad (18)$$

² $\perp\!\!\!\perp$ = linearly independent; \forall = for all; \Rightarrow = implies that

is obtained under randomization. I.e.: D_S does not change under randomization, *is a white noise* [94], and this is a property of the sequence of decimal digits of the sequence of digits of π . Randomization increases the Boltzmann entropy (Section 4.2 and equation (4–30) of [29]) or the algorithmic type [195, 120, 43] of a random sequence; a sequence maximizes its entropy or equivalently, or has a maximum entropy or information content [203, 188]. The conclusions could be falsified by assuming that the singularity in the infinite series functions used to calculate the digits [47] exist.

For more details on the decimals of π and its fractal dimension refer to the original work of Sevcik [183, 186], there. limited by the capacity of the available computers were calculated 10^9 of π decimal digits with the algorithm of Bellard [23], already by that time the maximum number of decimal digits of π known was 2.7×10^{12} digits calculated with the same algorithm [23]. At the time of writing this article $2,699,999,990,000 \approx 2,699 \dots \times 10^{12}$ decimals of π are known, [12], store that number of decimals requires ≈ 2.7 teraB of disk. But using 10^9 of decimals of π is enough to reach a value of $D_S \approx 1.888421 \pm 10^{-6}$ while a sequence of 10^9 decimal digits of type $U_{\mathbb{Z}}(0.9)$ decimal has a $D_S \approx 1.88743881 \pm 2 \times 10^{-6}$.

Since we do not know the distribution of the decimals of π , the approximation of the inequality of Vysochanskij–Petunin [213, 212, 214] was used to compare the diverse values of D_S obtained when the decimals of π studied were increased by taking the first in the sequence of $10, 100, 1000, \dots, 10^7, 10^8, 10^9$ π digits and a sequence of the same length of decimal distributed uniformly as $U_{\mathbb{Z}}(0.9)$ or $U_{\mathbb{R}}(0.1)$) versus the randomized sequence of the same number of π digits. However, when D_S was used to compare the sequence of π decimals with the same randomized sequence of π decimals and a sequence of the same length of $U_{\mathbb{Z}}(0.9)$ decimals, no statistically significant differences were found ($0.11 < P < 0.46$).

3.3. Other examples of the uses of D_S .

D_S used to analyze venoms was published (discussed below, [57, 60]), although perhaps the most important factor was that when Complexity International, where our work [184] was originally published, ceased to be active and the work was deposited in www.arXiv.org, [185]. With the use of www.arXiv.org, GoogleScholar starts tracking article usage (see <https://scholar.google.com/citations?hl=en&user=0VhfpTIAAAAJ>), but there are D_S uses that are unreported in GoogleScholar. We are aware of

multiple attempts to calculate D_{HB} and D_K before 2010, some of which are discussed here [74, 114, 72]

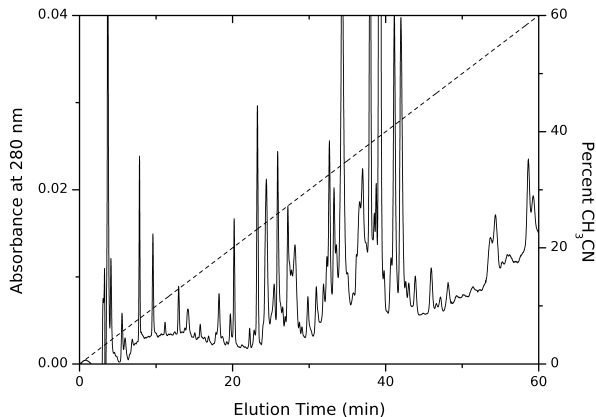


Figure 3: **Reverse phase high-performance liquid chromatography (HPLC) of *Tityus discrepans* scorpion venom.** HPLC separation of the water-soluble venom *T. discrepans* was made with a column of C_{18} of reverse phase, the data were acquired at a frequency of 1 Hz, so that 60 min represent a $n = 3600$ points. The chromatographic profile shown here corresponds to a batch milking of individual venoms, of 100 specimens of *T. discrepans*, put together as a lot poisons. For more details refer to the text of the book or the original publication [57].

3.3.1. Using D_S to compare complicated systems.

There are several situations where we consider complicated³ systems that we need to compare. An example appears when we need to compare the components that are separated in various chemical methods that are usually grouped under the name of chromatography. In these methods, a set of very diverse molecules are diluted in a liquid or gaseous medium that is forced to move through a solid medium, with which they interact and by that interaction, they separate forming “peaks” that are collected to study their properties.

One of the chromatographic techniques with the greatest capacity to separate compounds is the so-called high-performance liquid chromatography (HPLC), which separates components with different properties of electric

³The word “complicated” is used here to re preserve “complex” for numbers of type $(a + b\sqrt{-1}) \in \mathbb{C}$.

charge, molecular weight or polarity [197]. There is a huge number of examples of this analysis, here we will limit ourselves to consider the example of its use for the analysis of natural poisons (called ‘toxins’), produced by a genus of scorpions from South America, which we will arbitrarily limit to a genus called *Tityus* of which only in Venezuela more than 50 species [76] with great toxicity to humans are known.

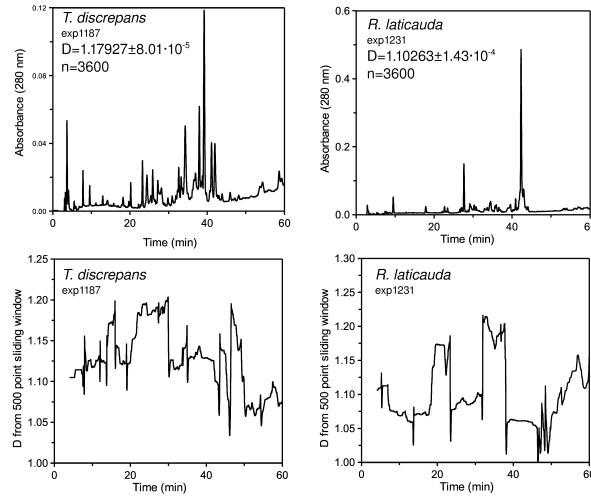


Figure 4: **Two sources for calculating the fractal dimension (D_S) of the elution pattern** . The figure presents data on the venoms of the scorpions *Tityus discrepans* (panels on the left) and *Rhopalurus laticauda* (panels on the right). The chromatography protocol is the same as that used in Figure 3. The top panel presents the pattern of elution an extraction (milking) of each venom of an animal of each species as ordered. Data were acquired at a frequency of $1Hz$, which is equivalent to $n=3600$. The bottom panel presents the fractal dimension D_S calculated for the upper traces and D_S was $1.17927 \pm 8.01 \times 10^{-5}$ [mean calculated with Eq. (10) and standard deviation as $\sqrt{\text{var}[(\int D_S)]}$ calculated with Eq. (15) for $n = 3600$ points of *T. discrepans*, and under the same conditions was $1.102637 \pm 1.43 \times 10^{-4}$, For *R. laticauda*. If you use a sliding window of n points it is possible to calculate $Q = D_s - 1$, assign that value to the center of the window and move it by 1 point, repeat the calculation of Q and assign it to the next point in the abscissa, and so on until the available points of the waveform are exhausted. This is what is presented calculated with a sliding window of $n = 500$ digitized points as explained for the upper panels, the value of D_S obtained from the first 500 points is assigned to the point $x = 250$, the window is offset by 1 point, it is recalculated and the value is assigned to the point with $x = 251$, and so on to the point $N - 250$. For more details refer to Figure 3, the text of the article or the original publication [57].

Here we will limit ourselves to consider the case of more impact, *Tityus*

discrepans that coexists with the largest city in the country, Caracas of 4 million inhabitants with about 5000 annual scorpion sting cases registered [57, 58, 59, 60], but which is only one of the localities affected by scorpionism by *Tityus* in Venezuela. From the venom of *T. discrepans* alone, some 206 fractions of toxic peptides [21] have been separated. The problem of the complexity of these poisons is highly relevant. To separate this large number of compounds, it is usually required to rechromatograph (repeat chromatography) under modified conditions the compounds obtained under the initial conditions.

Figure 3 presents the initial result of a chromatography of a batch composed of the milking of venom of 100 specimens of *T. discrepans*. A large number of chromatographic peaks are observed, and different peaks often have different effects, peaks that appear together in the chromatography profile usually have similar effects [59]. With elution profiles of such complexity, comparing poisons is complicated. And the complexity increases if one considers that the chromatographic profile varies between individuals of the same species, and varies seasonally as well.

Figure 4 presents the elution patterns of an individual (meang 1 milking from 1 scorpion)) milking of *T. discrepans* venom and an individual milking of venom of *R. laticauda*, a species of scorpion common in areas of Venezuela below 500 meters above sea level, which poses no risk to humans. The figure is an example that scorpions can be compared from individual to individual with HPLC, so an instrument for comparing individual chromatography is very useful. The upper panels of **Figure 4** show the chromatograms, *T. discrepans*, above and on the left, and *R. laticauda*, at the top right. Below each chromatogram is a graph of D_S calculated with a sliding window of 500 points in length, as indicated in the text of the figure.

Figure 5 is an example of using Q curves, such as those shown in the lower panels of the **Figure 4**. The figures were prepared by pairing point by point $\{Q_{i,1}\}_{i=1,\dots,N}$ with the points of $\{Q_{i,2}\}_{i=1,\dots,N}$ as ordinate. Which of the two sets was the abscissa and which ordinate, were arbitrary decisions of the experimenter. It is easy to conceive that if $\{Q_{i,1}\}_{i=1,\dots,N}$ and $\{Q_{i,2}\}_{i=1,\dots,N}$ were equal, the points on the graph would form a diagonal with slope 1. In the left panel of the figure, the sequence for *T. clathratus* was used as ordered, and *T. caripitensis* as abscissa. Although the correlation between the venoms is not perfect, the points are grouped around the line with slope 1 and intercept 0, is good enough to produce a coefficient of determination of 0.813. The graph on the left also has *T. caripitensis* as abscissa, but the

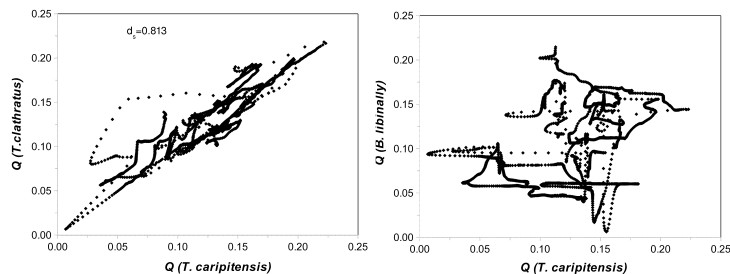


Figure 5: **Tortuosity graph constructed with a sliding window $Q = D_s - 1$.** In cases such as the elution profiles of poisons, the waveform to be analyzed is obviously not infinite. In such cases fractal dimension can be questioned, and it is preferable to use the ‘tortuosity’ component of the fractal dimension that exceeds that of a line. If a sliding window of $n = 500$ is used as explained for Figure 4, but here the set of $\{Q_{1,i}\}$ is plotted against the set $\{Q_{2,i}\}$, where 1 expresses one kind of scorpion and 2 the other; If both species were identical, the graph would be a line with slope 1 and intercept 0. The figure shows that *T. caripitensis* and *T. clathratus* have similar venoms, but that the venom of *Broteas libinalli* is very different from that of *T. clathratus*). For more details refer to Figure 4, the text of the book or the original publication [57].

ordinate corresponds to the venom of *Brotheas libinalli* D_S . The distribution of the points in the graph is far from its diagonal. The venom of *B. libinalli* offers no danger to humans. The graph suggests that the venoms of *T. clathratus* and *T. caripitensis* are very similar, and that the venoms of *B. libinalli* and *T. caripitensis* are very different. The reader interested in more detail should refer to the urinals studies [57, 60].

3.3.2. Fractal dimension of service queues.

There is an indefinite number of systems that provide services to an indefinite number of service seekers. Indefinite, here, has the same implication of \aleph_0 , an *indefinitely large* number fulfilling $\aleph_0 \in \mathbb{Z}$. Some services (the bus that passes at a certain time through my stop, the emergency of a hospital, the supermarket or pharmacy where I buy, etc.) are very obviously service provided to those demanding them. In all of them there is an obvious service provider, and a queue or line, of those waiting to be served. Perhaps less obvious as a service are public traffic means such as the, so-called highways. However, in all these cases the flow of those served follows a common function: a random Brownian march [35, 34, 180, 159, 154].

Four years ago I was consulted at the La FuenfríaMadrid Hospital, a

hospital of the Madrid Health Service (SERMANS) dedicated to treating chronic cases. The reason for the consultation was to increase the efficiency of the Hospital, prone to prolonged periods of low occupancy. Full data was published [179] and we refer interested readers to that publication for details omitted here. For the analysis, daily Hospital occupancy data from May 1, 2014 to December 19, 2017 [179, corrections for asymmeter errors as indicated here].

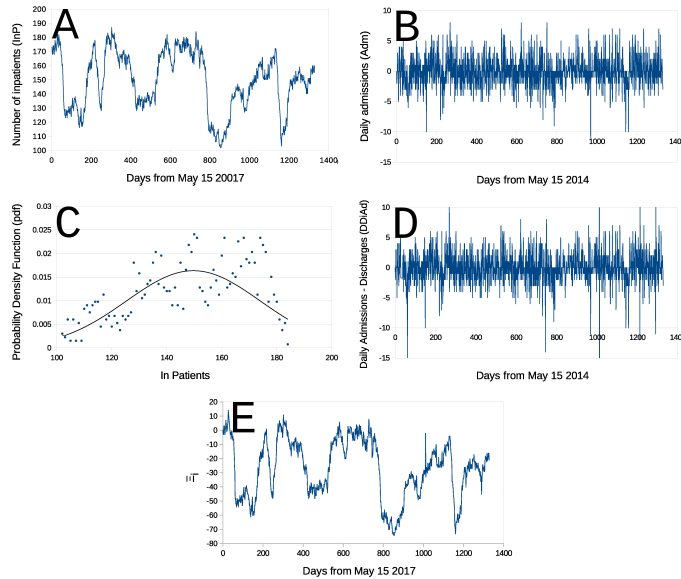


Figure 6: **Patients hospitalized every day (InP) at La Fuenfría Hospital from May 1, 2014 to December 19, 2017.** The panels are: **Panel A-** Number of hospitalized patients (**InP**) at Hospital La Fuenfría on each day of the Hospital study; **Panel B-** Daily variations (**DInP**) of patients staying at Hospital [Δ and in Eq. (19)]; **Panel C-** Panel A data expressed as *f*umtion of *density* of probability (*fdp*), the probability of observing a measurable or countable random event) for any number of patients (**InP**) who remain hospitalized each day during the study period (\bullet) [217], a Gaussian line of type ($N[\bar{y}, s[y]]$) with mean \bar{y} and variance ($s[y]^2$) both calculated for the 1329 data in Panel A ($\bar{y} = 149.2$ and $s[y] = 24.4$); **Panel D-** Daily differences between admissions (**Figure 7A**) and hospital discharges (**Figure 6C**) at the Hospital (**DDiAd**). **Panel E-** Random march Ξ_i built for **DDiAd** (Panel D) using Eq. (20), please note that the end resembles the **InP** sequence in Panel A. In all cases abscissa is the number of days between May 1, 2014. The largest negative or negative peaks are off-scale from the charts.

With the Hospital data, a sequence of values of Δy_i was constructed as

indicated in the following equation:

$$\Delta y_t = \begin{cases} 0 & \implies t = 0 \\ y_t - y_{t-\Delta t} & \implies t > 0 \end{cases} \quad (19)$$

Here the y_i are daily data and the Δy_i are the daily changes, of the various occupations of patients in the Hospital. The **Figure 6A** shows the sequence Δy_t calculated with the Eq. (19), the curve covers a total of 1216 days of study. During the study period, the number of hospitalized patients was 150 (149–151) (median, and a 95% CI, $n = 1329$ days) in a range of (102–187) patients, meaning that Hospital occupancy is 0.77 (0.53–0.77) (median, and, its 95% CI). There could be one 4 “cycles” where the curve goes from 60% from occupancy to a total of 98% occupancy in a “cycles” of about 304 days (≈ 10 months) duration?. If we accept those “cycles” as real, they do not follow any annual seasonal period that we could identify. something that is, at least, rare.

Figure (6)C is a graph of the pdf of daily variations of the data in **Figure (6)A**, there it is observed that the data are not Gaussian, there are no negative data and there is a skewness towards positive high values.

Trying to understand **Figure 6A** we built **Figures 6B** and **6D**. The first of these (**Figure 6B**) is the number of patients the Hospital receives daily, and the second (**Figure 6D**) is the number of patients the Hospital discharges (patients leaving the Hospital) daily. From the simple observation of the data in **Figures 6B** and **6D**, there does not seem to be a pattern in them, they look like two “white noises” [94], random oscillations around a mean, which are commonly distributed in Gaussian form.

It is surprising, however, that if we calculate the daily difference between input and output and graph them, we obtain the **Figure 6E**. This figure is constructed as the Ξ_i of the **Figure 6E**, Built with Eq. (20):

$$\Xi_i = \begin{cases} 0 & \implies i = 1 \\ DD_i Ad_i + \Xi_{i-1} & \implies 2 \leq i \leq 1328 . \end{cases} \quad (20)$$

Surprisingly, with the exception of a few peaks that go out of the curve, probably resulting from the subtractive cancellation of small differences, the **Figure 6E** is almost identical to the **Figure 6A**. The fundamental difference between the curves in the **Figures 6B** and **D** is that they reflect a delay in admitting a patient to the Hospital after another has been discharged,

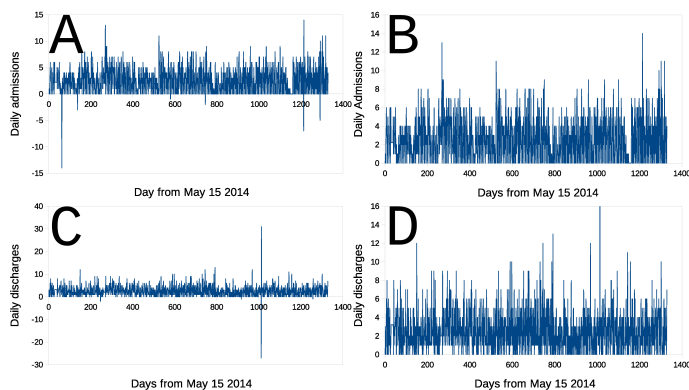


Figure 7: **Sequences of admissions and daily discharges from La Fuenfría Hospital.** The Panels are: **Panel A-** Hospital Daily Admissions Sequences (**Adm**); **Panel B-** Same as panel A, but changing the scale to display data ≥ 0 ; **Panel C-** Sequence of daily discharges (**Dis**); **Panel D-** Same as Panel C, but scaled to include only data ≥ 0 . In all panels, abscissa is the days elapsed since May 1, 2014, and the ordered abscissa is the daily number of patients admitted or discharged. Negative spikes represent transcription errors of data that were available for study, positive extreme data probably have the same, see original reference for more data [179].

this shows the original work of Rodríguez-Hernández and Sevcik [179, Check Figure 4]. The Figures 6E and 6A are practically identical, and belie the idea that the apparent “cycles” are due to some seasonal factor external to La Fuenfría Hospital or the SERNAS hospital network of which the Hospital is a part. And more, the data favor the hypothesis that the oscillations of the occupation of the Hospital La Fuenfría, is due to factors that determine a delay in admitting a patient when another is discharged, not to some hidden factor external to the Hospital, or in the best of cases to the hospital network of SERMAS.

In **Figure 7** it becomes more evident that income and discharges have a positive median (**Figure 7B and D**) when a few negative data likely resulting from subtractive cancellation between small data are deleted (**Figures 7A and 7C**).

The relationship between **Figures 6A** and **6E** can be understood if one uses Monte Carlo simulation to generate data around a known pdf and Markovian time series [151, 192]. In principle, we can visualize two kinds of time series where data that have a pdf appear such as $y_i = g(x_i | \{\theta\})$, where $\{\theta\}$ is a set of parameters on which y_i depends. Then we can conceive of a series

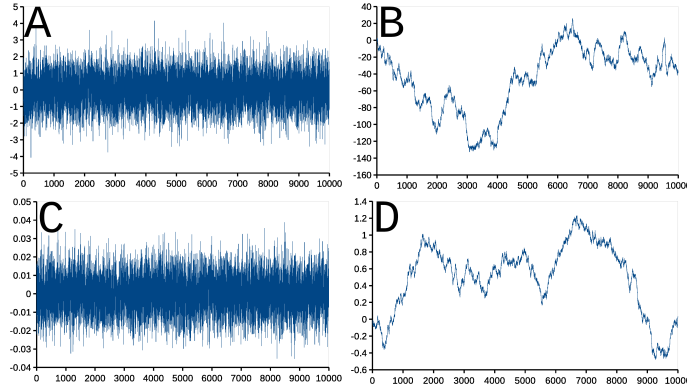


Figure 8: **Two white noise sequences generated with Monte Carlo simulations [Panels A and C], as indicated by Box and Muller [31, 172].** The Panels are: **Panel A**, Gaussian White Noise and **B**: Gaussian Brownian Noise Rw , generated using Eq. (23) forms the data in panel A; **Panel C**, Gaussian white noise and $\{g_i = \mathbf{N}\{0, 10^{-4}\}\}_{i=1,2,\dots,10^4}$; **D**: Rw Gaussian, generated using the Eq. (23) with panel C data, the abscissa and ordinate are arbitrary. Please note that $[D_S \pm s(D_S)]$ estimated with Eqs. (10) and (15) are: Panel A, $1.66122 \pm 7.60191 \cdot 10^{-4}$; Panel B, $1.32692 \pm 7.6926 \cdot 10^{-4}$; Panel C, $1.6692 \pm 7.64176 \cdot 10^{-4}$; Panel D, $1.31723 \pm 7.72806 \cdot 10^{-4}$. Rw is a *random walk*, of the original work. See the original reference and text of this book for more data and details [179]

such as:

$$y_i = g(x_i | \{\theta\}) \quad (21)$$

$$y_i = y_{i-1} + g(x_i | \{\theta\}). \quad (22)$$

In the first case any point $(y_j \perp y_i)_{\forall(i \neq j)}$ ⁴, is a waveform we call white noise. In the second case $(y_i \not\perp y_j)_{\forall(i \neq j)}$, but we cannot say how, this is what is called a Markovian process or a Markov series, the sequence that constitutes the waveform is usually called Brownian noise, since that kind of movement was discovered in the nineteenth century as characteristic of pollen grains in liquid medium by Brown [35, 36]. In white and Brown noises of the most common type, however, the pdf is Gaussian such that $g(x_i | \{\theta\}) = \mathbf{N}\{\mu, \sigma^2\}$, with mean μ and variance σ^2 . Brownian noise follows a function as:

$$b_i = \begin{cases} b_1 = 0 \\ b_i + g_{i-1} \end{cases} \implies 2 \geq i \geq 1329. \quad (23)$$

⁴ \forall means ‘for all’

Please note that **Figures 8A** and **8B** were calculated with Eq. (23) are plotted with **exactly the same set** $\{g(x_i | \{\theta\})\}$ obtained from the Monte Carlo simulation, just as **Figures 8C** and **8D** do with yours.

This type of noise in its white and Brownian version, also referred to as Brown noise, is presented in the **Figure 8**. **Figures 8A** and **8B**, are white and Brown noise with a pdf $\mathbf{N}\{0,1\}$ and the **Figures 8C** and **8** with $\mathbf{N}\{0,10^{-4}\}$. Note that if you look at the **Figures 8A** and **8C**, or the **Figures 8B** and **8D** without noticing the ordinate scale or variances noted above, one of those pairs looks the same as each other; the same goes for **Figures 8B** and **8C**; These similarities are the so-called self-similarities or self affinities of fractal processes, which in the case of white and Brown noises determine that they look the same at any scale of the abscissa that are observed. Note that despite the differences in their $g(x_i | \{\theta\})$ figures **8B** and **8D** look very similar to each other and to **Figures 6A** and **6E**.

The fractal dimension $D_{HB} = 2$, for a white noise and is $D_{HB} = 1.5$ for one Brown noise [94, 184, 185, 186]. Rodríguez-Hernández and Sevcik [179] showed that $D_S \rightarrow 2$ for **Figures 8A** and **8C** when the sequences lengthen towards \aleph_0 and that at the same time $D_S \rightarrow 1.5$ when the noise sequences **Figures 8B** and **8D** are also lengthened. Rodríguez-Hernández and Sevcik [179] is therefore a demonstration of the existence, perhaps unsuspected, that in the operation of a modern hospital, there may be hidden factors, which make it behave like most service providers as a queue in contemporary literature in English), which in this case determines periods of low use of the Hospital, which can be considered “inefficiency” but which are not soluble if the hospital network of Madrid en bloc is not considered, not as individual hospitals of SERNAS. Please review the original work [179] for more details.

3.4. Higuchi’s fractal dimension.

In the fractal literature [94] there are two ways to approximate the fractal dimension of a waveform. One of them is the use of open circles that cover the curve, this we have discussed in relation to D_S [184, 185] where a double linear transformation to a unit square is used. The other is the use of “open boxes” that cover the wave, those boxes are usually squares of side d . Long ignored by the authors, there is another form of fractal dimension estimation using boxes, developed by Higuchi [98, 99]. It is called fractal dimension because the waveform whose fractal dimension is to be estimated is covered by “boxes”, actually, in two dimensions, *squares* of side d . As follows from

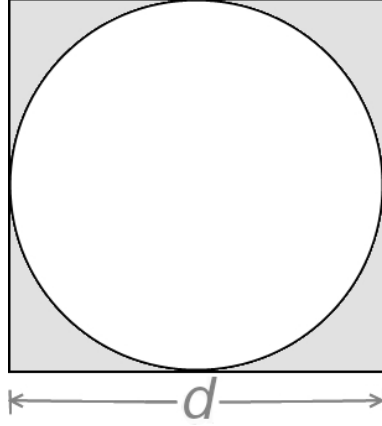


Figure 9: **The relationship between open boxes and open circles to calculate the fractal dimension of a curve.** If we call ϵ to the radius of the circle, then the side of the square will be $d = 2 \cdot \epsilon$. Please note that the lines have been drawn very thickly, they should be points of radius $\epsilon = \frac{d}{2} \rightarrow 0$ and the outermost layer of points, in an “open” square or a circle, are not included in the respective square or a circle. From the figure it is intuitively obvious that, except for possible segments of a curve parallel to the abscissa or the ordinate of the curve, it will take fewer squares than circles to cover the curve since $d^2 > \pi \epsilon^2 = \pi \left(\frac{d}{2}\right)^2 \iff 1 > \frac{\pi}{4}$. Where ϵ is used as in Eq. (6) and subsequent ones.

Figure 9 it takes more circles than squares to cover any waveform other than a vertical or horizontal line. In other circumstances $D_{\blacksquare} \lesssim D_{\bullet}$. Here we use a slightly different notation than Higuchi [98], using matrix notation. To understand the fractal dimension of Higuchi [98, 99] we will consider a time series of observations such as

$$\{x_1, x_2, \dots, x_N\}. \quad (24)$$

From this sequence we will construct a subsequence such as

$$\begin{aligned} \{X_k^m\} &= \left\{x(m), x(m+k), x(m+2k), \dots, x\left(m + \left[\frac{N-m}{k}\right] \cdot k\right)\right\}_{m=1,2,\dots,k} \\ \therefore \{X_k^m\} &= \{x(m), x(m+k), x(m+2k), \dots, x(N)\}_{m=1,2,\dots,k} \quad \square \end{aligned} \quad (25)$$

The deletions of the last term in Eq. (25) are mine.

Here Higuchi introduces a condition that he does not explain, this is that the term in square brackets, there is none other than $\left[\frac{N-m}{k}\right]$, “denotes Gauss’s notation” (there is no other explanation about Gauss suggesting that) and that both k and m are integers [we presume that it means $(m \in \mathbb{Z}) \wedge (k \in \mathbb{Z})$] and points out that m and k indicate the initial time and the time interval (Between the points?)

respectively. Starting from that series Higuchi [98] constructs the following matrix of equations, for say $N = 100$:

$$\begin{aligned}\{X_1^3\} &= \{x(1), x(4), x(7), \dots, x(97), x(100)\} \\ \{X_2^3\} &= \{x(2), x(5), x(8), \dots, x(95), x(98)\} \\ \{X_3^3\} &= \{x(3), x(6), x(9), \dots, x(96), x(99)\}\end{aligned}\quad (26)$$

Higuchi [98] *defines (without explanation)* the length of each curve $\{X_k^m\}$ as follows:

$$L_n(k) = \frac{\sum_{i=1}^{\frac{N-m}{k}} |x(m+i \cdot k) - x(m-(i-1) \cdot k)| \cdot \left(\frac{N-1}{\left[\frac{N-m}{k} \right] \cdot k} \right)}{k} \quad (27)$$

$$L_n(k) = \frac{N-1}{\left[\frac{N-m}{k} \right] \cdot k} \cdot \sum_{i=1}^{\frac{N-m}{k}} |x(m+i \cdot k) - x[m-(i-1) \cdot k]| \quad (28)$$

Eq. (27) in its first form is the Higuchi curve length equation with more contemporary notation, Eq. (28) is the same, simplified to make it more understandable and compact. If the original publication [98] is reviewed, there is no explanation about the two vertical lines that limit the term within the sum of the Eqs. (27) or (28), the journal where the article was published had no problem representing parentheses, braces or brackets of any size, as is obvious in Higuchi's article [98] itself, so that these unexplained vertical lines can only be considered as indicating that the summation is made over the *absolute values* of the differences within the summation. This is strange, assuming p_i and p_{i+1} are point in a two dimensional Euclidean space with coordinates (x_i, y_i) and (x_{i+1}, y_{i+1}) , respectively. The distance between p_i and p_{i+1} , according to the Pitagoras theorem will be $\sqrt{(x_{i+1} - x_i)^2 + (y_{i+1} - y_i)^2}$ and the absolute value function is never necessary.

According to Higuchi [98], the fraction $\frac{N-1}{\left[\frac{N-m}{k} \right] \cdot k}$ represents the “*normalization of curve length*” of a “*time series subsystem*”. Also, according to Higuchi [98]: the length of the curve is defined for the time interval “ k , $\langle L(k) \rangle$ ”, as the average value of the parameter k of the sets $L_m(k)$. Again according to Higuchi [98]: if

$$\langle L(k) \rangle \propto k^{-D_{Hig}}, \quad (29)$$

the fractal dimension of the curve is D_{Hig} ⁵.

Thus the fractal dimension is a constant of proportionality between k , the abscissa and $L(k)$, the ordinate, the relationship between them is an exponential. The idea, however, is not original to Higuchi

⁵The subscript *Hig* is mine

Higuchi [98] validated his method to determine the fractal dimension tests with “simulated data” to which he applied his method. First, he applies his technique to the simulated data $\{y_i\}_{i=1,2,\dots,N}$ with fractal dimension $D = 1.5$, y_i is generated as

$$y_i = \sum_{j=1}^{1000+i} z_j \quad (30)$$

where z_j is *is assumed* Gaussian with mean 0 and variance 1 [98]. “The value of 1000 was taken arbitrarily to eliminate the effect of arbitrarily sampling z_i for y_1 ” [98]. Higuchi used the following values for the interval $k = 1, 2, 3, 4$, and $k = \left(2^{\frac{j-1}{4}}\right)_{j=11,12,13,\dots}$ for $k > 4$, “where Gauss notation” (*sic*, I don’t know what Higuchi means), here Higuchi is inconsistent now uses ($k \in \mathbb{R}$), observe that $k = 2^{2.5} = 5.65685\dots$, for example.

Then, if $\langle L(k) \rangle$ is plotted against k on a logarithmic double scale, the data must fall on one on a line wcon slope $-D_{Hig}$ (here we deviate from Higuchi, in the terms after the implication),

$$\log(L(k)) = -D_{Hig} \log(k) \xrightarrow{\text{con suerte}} \quad (31)$$

$$D_{HB} = \lim_{d \rightarrow 0} D_{Hig} = - \lim_{d \rightarrow 0} \left[\frac{\log L(d)}{\log(d)} \right] = - \lim_{d \rightarrow 0} \log_d [L(d)]$$

which is a form of Eq. (29) changing the proportion to equality, which means that any difference produced by this change falls within Higuchi’s D . The d is entered with the same sense as it has in the **Figure 9**. I introduce the implication because Higuchi simply calls ‘fractal’ his D [98], and it is Mandelbrot [139, pg. 15 and Ch. 39] who invents the term “fractal”, and associates it with the Hausdorff-Besicovitch dimension [95, 27]. The “luck” referred to indicates the lack of *formal* association between D_{Hid} and D_{HB} that is not formally established anywhere by Higuchi. Higuchi [98] simply *defines*: $D_{HB} = D_{Hig}$.

Higuchi [98, pg. 280] gives an example of his definition of length in relation to Burlaga and Klein’s description [37] of these authors’ fractality of the interplanetary magnetic field, as follows

$$\begin{aligned} L_{BK}(3) = \frac{1}{9} [& |(x_4 + x_5 + x_6) - (x_1 + x_2 + x_3)| \\ & + |(x_7 + x_8 + x_9) - (x_4 + x_5 + x_6)| \\ & + |(x_{10} + x_{11} + x_{12}) - (x_7 + x_8 + x_9)| \\ & \vdots \\ & + |(x_{\aleph_0-2} + x_{\aleph_0-1} + x_{\aleph_0}) - (x_{\aleph_0-5} + x_{\aleph_0-4} + x_{\aleph_0-3})|] \end{aligned} \quad (32)$$

which was here rearranged here to make it more compact and understandable. Note that in the last term the expression up to \aleph_0 is explicitly presented (to say

a cardinal as large as you like). The original version of Higuchi only says “+ . . .)” where a bracket seems to be missing. Then the same definition, with apparently the same errors, is repeated for $\langle L(k) \rangle$. All definitions of Higuchi are strange. It is not stated, for example, why in $L_{BK}(3)$ (Eq. 32) or $\langle L(k) \rangle$ (Eq. 28) the whole sum is divided by 3 (. . . /3 at the end of each of those expressions) and each of the terms of the sum is divided by 3 as well, nor why division by this constant is not taken as a common factor of the sum to simplify it. In my transcription (Eq. 32) of the Higuchi equation I extracted them and placed them as $\frac{1}{9}$ before the sum of the differences of the absolute values but I guess that $\frac{1}{3}$ would be more correct.

Another incomprehensible thing is why Higuchi uses the absolute value of the differences between neighboring points to calculate the length $L(k)$ of his curves. If these curves are constituted (away from Higuchi’s notation) by a set of data pairs $\{x_i, y_i\}_{i=1,2,\dots,N}$ then the length of the curve will be

$$\mathcal{L} = \sum_{i=2}^N \sqrt{(y_i - y_{i-1})^2 + (x_i - x_{i-1})^2}$$

according to the Pythagorean theorem $L = \sum_{i=2}^N |y_i - y_{i-1}|$, as Higuchi seems to use [98], so that $\mathcal{L} > L$, which means that Higuchi [98] underestimates the length of the curve’s fractal dimension it claims to estimate, unless the author uses the two vertical bars as something distinct, and unexplained.

3.4.1. A final word on Higuchi fractal dimension.

The logarithms of waveform’s length at a long time, $\log_b \langle L(k) \rangle$ (b is any basis), for a time series, y_i with $N = 217$, is plotted as a function of $\log_b L(k)$ in Figure 1 of Higuchi [98]. This appears to be a kind of Monte Carlo simulation of a Brownian noise like the one shown and discussed in **Figure 8B** and **8D**, but does not give any information about the reliability of the generator of a random variable such as $\mathbf{N}\{0, \sigma^2\}$ and today would not be considered acceptable for publication [184, 185, 183, 179]. Higuchi [99] makes a second publication with his method, in it he cleans up algebra somewhat and makes it less baroque. But again the 1990 [99] publication he does what looks like a Monte Carlo simulations which is not described. They have been described for today’s requirements. Monte Carlo, it seems. After the work of 1990 [99], the use of the “fractal dimension of Higuchi” disappears from the literature (in my experience) until the year 2004 when it reappears, and is used used mainly in medicine, without any additional formal analysis [2, 56, 218, 198, 199, 92, 1, 50, 127, 128, 187, 8].

Thus, ways of estimating D for curves in two-dimensional Euclidean spaces began to appear developed by Higuchi [98, 99] and by Katz [116]. Both of Higuchi’s papers were published in *Physica D: Nonlinear Phenomena* [98, 99], backed by

another Japanese physicist. As we discussed earlier, the papers by Higuchi [98, 99] are strange. The first paper with a “muddy” algebra and many unexplained *definitions*. Higuchi’s method, then, disappears from the literature for 15 years and is cited again after 2004 [2, 218, 92, 1, 50, 129, 187, 8], some of these references include attempts to validate Higuchi’s dimension [129].

4. Frequency analysis as a form of data analysis.

Another interesting way for data analysis of time series, used for example in Rodriguez-Hernandez and Sevcik [179], is frequency analysis. Frequency analysis is not part of the analysis of chaotic or fractal systems, and also includes strictly statistical time series concepts such as autocorrelations and autocovariances. We will continue to use the work [179] as an example of this analysis. se can refer to [158, 25, 196] among others.

A classic way to show periodicities of mathematical functions in the time domain is to transform them to the frequency domain, which is a sum of sines and cosines, using a fast Fourier transformation (FFT) [28, 216]. The transformed values for each frequency (f) are “complex numbers”, $c_f \in \mathbb{C}$, with two components: one of them is some class sometimes called simply “real component” such as $a_f \in \mathbb{R}$ and a $b_f \in \mathfrak{I}$ component called “imaginary”. A complex number has the form

$$c_f = a_f + b_f\sqrt{-1} = a_f + b_f\mathbf{i} \implies \begin{cases} c_f & \in \{\mathbb{C}\} \\ a_f \wedge b_f & \in \{\mathfrak{R}\} \\ b_f\mathbf{i} & \in \{\mathfrak{I}\}, \end{cases} \quad (33)$$

where parameters indicate sets of numbers, and \in reads “*belongs to*”. The “energy”, expressed as a stable nonzero curve, or as increases in sharp peaks or variations in amplitude (such as the peak in the **Figure 10B**, this is called “spectral density” (ψ_f) and, sometimes, we might informally call as the “weight”), contributed by each frequency component to the energy of the total signal in a complicated process that fluctuates and is expressed as

$$\left(\psi_f = \sqrt{a_f^2 + b_f^2}\right) \in \mathbb{R} \quad (34)$$

If you plot ψ_f against f you get a a spectral density graph, which is a set of real numbers ($\{x_i\} \in \mathbb{R}$). An intuitive way to understand this is to consider a perfectly periodic signal such as a sinusoidal trigonometric series such as a sine function $\zeta(x) = \sin\left(\frac{2x\pi}{T}\right)$ where $\pi = 3.1415926\dots$ and T is a constant (called *period*) that has the same units (meters, seconds, grams, volts, or any other) that has x . An example is shown in **Figure 10A**. **Figure 10B**, presents the power spectrum of **Figure**

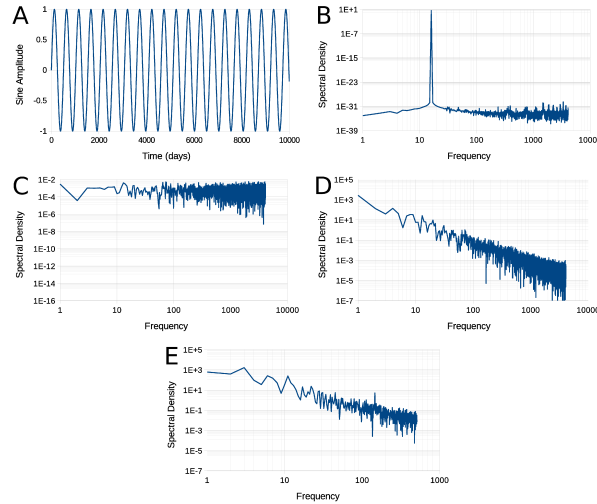


Figure 10: **Analysis of the false periodicity of Rws . Using spectral density analysis (ψ_{f_j}).** The panels are: **Panel A**- A perfectly periodic signal, the trigonometric function $\zeta(x) = \sin(x \frac{\pi}{128})$; **Panel B**- ψ_{f_j} of the sine function displayed in panel A; **Panel C**- ψ_{f_j} of white Gaussian noise shown in Figure 8A; **Panel D**- ψ_{f_j} of Brown's noise [94] Rw shown in Figure 8B; **Panel E**- ψ_{f_j} of the sequence of hospitalized patients (InP) that appears in the **Panels A** up to **E** of **Figure 6A**. The ordinate of the panels from B to E, is the power dissipated at each frequency. The function shown is the displayed sine function presents the dissipated energy all its energy in a single peak ψ_j (Panel B). The *sequence for the number of hospitalized patients SDf_j corresponds to a Gaussian Rw without any underlying periodicity.* All graphics SD were fitted a window of Hann [28, 93]. The rapid oscillations observed to the right from **Panel B to D** are artifacts due to the sampling of discrete points, in the signal to perform the Furrier transformation. Rw is used in the original work cited as *random walk*, more details in the text of this book and the original work cited [179]

10A consisting of a single peak with frequency $f = \frac{1}{T}$. Please note that calculating ψ_f the actual signal is sampled at intervals of Δx (equivalent to multiplying by something called *Dirac comb* and the FFT also contains the frequency content of the Dirac comb produces the burst of high frequency vibrations of vibrations the right half of each stroke [28].

Figure 10C is a spectrum ψ_f of Gaussian white noise shown in **Figure 8A**; the ordering of panels from **8B** to **8E**, in arbitrary units. In **Figure 10C** it is observed that all frequencies have the same “weight”, that is, all frequencies contribute equally. **Figure 10D** is a spectrum Rw of a Brownian noise ψ_f ; On the logarithmic double coordinate scale, the spectral density line is a decaying line with a slope of $\frac{1}{f^2}$. **Figure 10E** is ψ_f of patients hospitalized each day (InP in

the figure) is shown in **Figure 6A**.

Even though the simulated sequences in **Figure 10** are only 10000 points and those in are only 1329 points long, there is an obvious similarity between the Brownian noise ψ_f (**Figure 10D**), and ψ_f of the sequence of patients in the Hospital (*Inp*) between May 1, 2013 and December 19, 2017 (**Figure 10E**). In cases ψ_f are characteristic of the Brownian noise Rw and none of these ψ_f s have peaks that could indicate a suggestion of any periodic component which could some periodicity, despite short lapses or long Brownian lapses the Rws that could give this impression.

Figure 10C is a Gaussian white noise ψ_{f_j} calculated for the signal in **Figure 8A**. In **Figure 10C** all frequencies have the same “weight”, the contribution of all frequencies is the same, “white” for this kind of noise. **Figure 10D** shows ψ_{f_j} of the Brownian noise Rw in **Figure 8B**, it can be seen that with logarithmic double coordinates the spectral density follows a straight line that decays with a slope of $\frac{1}{f^2}$. Finally, also in **Figure 10E**, ψ_{f_j} is shown which corresponds to the sequence of daily hospitalized patients **Figure 6A**. Except for the simulated sequences in **Figure 10** where 10^4 points are simulated and for Hospital data where they are 1329 points in length, there is an obvious similarity between the Brownian noise ψ_{f_j} , and the ψ_{f_j} of patients discharged from the Hospital between May 1, 2013 and December 19, 2017. In both cases ψ_{f_j} are characteristic of a Rw and *none of those ψ_{f_j} has some suggestive peak of periodic components that could explain any periodicity, despite short periods in Rws that seem to suggest it.*

Since Mandelbrot introduced the concept of ‘fractal’ and published his “Fractal Geometry of Nature” [137, 139, 144] the notion of fractal dimension and fractal geometry have invaded virtually every corner of the economy [139, 142, 222, 223], medicine [171, 46, 176]. Multiple corners of biology [94], epidemiology [150, 184, 185], physics, service systems [208, 179], seismology [64, 41, 205, 204], the study of reversible reactions and enzymes [182, 220] and much more, including so called multifractal systems with more than one fractal component [122, 223, 114, 194, 85, 124, 123].

5. Parameters once related to the fractal dimension: The Hurst exponent.

5.1. The Hurst water source model.

Mandelbrot [139, 94] has pointed out, that the fractal dimension is related to previous concepts associated with, for example, the flow of rivers, which would be an interesting natural phenomenon *per se*. This would be the case, of the flow of the Nile River. Harold Edwin Hurst (1880 – 1978) a British hydrologist [201, 202, 160, 200] who was dedicated to measuring the level of the Nile river

since 1906, for 62 years. Hurst published his first paper in 1951, one of the most influential and highly cited works in scientific hydrology, [107], he was then 71 years old. Hurst's nomenclature is not easy to follow, since almost all of his variables are single letters hinting nothing about their meaning. The work of 1951 is followed by other papers in 1956 [108, 110, 109].

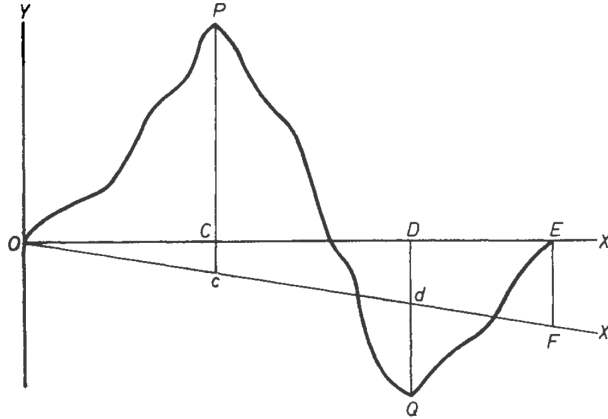


Figure 11: Credits of the figure in Recognitions [109].

Hurst [109] recorded the level of the Nile, since 1906 ($\cong 44$ years) preceded by about ≥ 2000 [109, Table 2 and Figure 1] years of historical records. If we assume that the flow of the Nile enters a reservoir of indefinite capacity, from which there is a constant efflux equal to the annual average of discharge (evaporation, irrigation, consumption, etc.). The storage that would be required to make the discharge flow of each year is obtained by computing the *continuous sums of the annual deviations from the mean*. Then the range R between the maximum and minimum of these continuous sums is either: (a) the maximum storage when there is no deficit, (b) the maximum accumulated deficit when there has never been maximum storage or (c) its sum when there is storage and deficit.

Suppose we have a record of the annual discharges of a river over a number of years, and we assume that the river flows into a reservoir of indefinite capacity, from which there exists a constant influx equal to the mean annual discharge.

The storage required for the annual discharge to flow is obtained by adding the excess water to the average. Then the range R from maximum to minimum of the continuous sums is either: (a), the average accumulated storage when there is never a deficit; (b), the maximum accumulated deficit when there is never a water accumulation; or (c), the sum when there is accumulated and deficit water. In Figure 11 (or [109, pg. 14]),

$$R = (P - C) + (D - Q). \quad (35)$$

This is shown in **Figure 11** [109, **Figure 1**] where $X \in (0, X_{max})$ is the time axis and $Y \in (-Y_{min}, Y_{max})$ is the *axis of accumulated departures from the mean* $M = \bar{Y}$, of Y . The curve expressing this transitions, in sequence, through the points $0 \rightarrow P \rightarrow Q \rightarrow E$, and $Q \rightarrow E$ ⁶. *N is the number of year of observation* [109, pg. 14]. During the period $0 \rightarrow C$ the deviations from the mean are positive and the damn storage or river level of the interval, increases from $0 \rightarrow P$. Then $C \rightarrow D$ period, represents a reduction in water storage in period $P \rightarrow Q$, which determines that the curve reaches a negative level with respect to the mean storage and then returns to the mean value $Q \rightarrow 0$ in the $D \rightarrow E$, period. $P \rightarrow C + D \rightarrow Q = R$, and this amount of storage would have allowed the average discharge of the period to have been maintained during it. The point F whose ordinate is $E - F = [-N(M - B)]$. Hurst notation is, generally speaking awkward, B is water draft which is $B < M$ [109, pg. 19]; F is thus an indicator of water overdraw.

5.2. The development of the Hurst coefficient.

Hurst [109] usually *assumed* that the flow distribution of rivers approximates a “normal” or Gaussian curve wit mean μ and variance σ^2 , or $N\{\mu, \sigma^2\}$, and that this is usually true, but that it is only part of the description of the phenomenon, since there is also a tendency to exist for high and low years that are grouped together. As far as I know, he never performed any valid statistical analysis to support this Gaussianity assumption. “*Theoretical research shows that, if individual years were completely independent of each other and each year’s discharges were completely independent of each other and discharges, the most likely value of $R \mid \sigma$* ⁷ would be given by” [109]

$$R \frac{R}{\sigma} = \sqrt{\frac{\pi}{2} N} = (1.25 \dots) \cdot \sqrt{N}, \quad (36)$$

where, as said, *N is the number of years of observation* and σ is the standard deviation of discharges for the period considered. Experiments with random events such as flipping coins agree with this equation.

Records of discharges from a number of rivers were examined and R was calculated for as many of them as were available. Unfortunately, no records were then found of discharges from a river covering more than 70 years, and therefore R was computed for a number of rainfall records of which several spanned more than 150 years. To these were added some records of various river levels, temperatures, and pressures. A common feature of all records was that their frequency distributions, ignoring the order in which they occurred, were of the rounded type to approximate

⁶ \rightarrow is used as “approaches” or “tends to”.

⁷ \mid means “given”.

the curve of the Gaussian normal distribution. When R was plotted as a function of N the equation produced an elongated group of points

$$\frac{R}{\sigma} = 1.61\sqrt{N}$$

In this group there was nothing to distinguish one type of phenomenon from another, but it was clear that that R was increasing faster than was the case with random events. This was attributed to the tendency of natural phenomena to have runs when the values as a whole are higher values and others were low. Due to the dispersion of points whose length of available records was not large enough to decide whether $\frac{R}{\sigma}$ for natural phenomena was better represented by the square root or by some other function of N .

In the attempt to resolve this point longer records of rainfall, temperatures, pressure, and lake levels continued to be computed for longer natural periods of natural phenomena. as a result the analysis was extended to the records of the Nilometer of Roda (Cairo, Egypt), which went back, with discontinuities, to the year 640 BC, the thickness that produced records up to 900 years, and clay tablets from which 4,000 years of record were available.

In total, 75 different phenomena were used. In the case of three rings results from 4 different locations were considered separately, and the findings were separate, and the findings were used for each locality are the means of a group of approximately 10 trees . A record was divided into periods and for each of them the $\frac{R}{\sigma}$ was compared. For example, with 120 years recorded it can be calculated for 3 periods of 40 years, two covering periods of 80, and a full period of 120 years. In general R was computed for periods of less than 30 years, in total 690 values of $\frac{R}{\sigma}$ were used. A preliminary long-term examination of the data showed that $\frac{R}{\sigma}$ increased faster than \sqrt{N} and less rapidly than and N . To find the form of the relationship the statistics were divided into sets containing similar phenomena, and the sets were again divided into groups, each group consisting of a small number of values of $\frac{R}{\sigma}$ with approximately the same value of N . Hurst [109] tabulates these values in his Table 1 as means of $\frac{R}{\sigma}$ together with N and its logarithms. Figure 2 of Hurst [109] presents the $\frac{R}{\sigma}$ plotted against $\log(N)$ to produce 7 good linear regressions.

A striking point of the discussion that Hurst in all his works, is that he uses concepts such as *media*, *deviation from the mean*, *standard deviation* (σ) or “Gaussian” without any explanation or justification. It seems to mean data distributed with a pdf such as $\mathbf{N}\{\mu, \sigma^2\}$, which should be distributed symmetrically around μ , however that symmetry does not exist in our **Figure 11** [109, Original Figure 1] or in any equivalent figure in any Hurst work. As stated above, if the median and 95% CI are calculated for the 11 values of K in the in the [109, Table 1],

there is an asymmetry between the medians and their 95% CI for the values of K , even though we do not place the values here because the samples become small, the asymmetry also exists for the sets of \mathbf{K} separating the data of $\mathbf{N} = \mathbf{114}$ and $N = 25$ from [109, Table 1]. This probably ignorance of Hurst and the tendency until the first half of the twentieth century to consider all Gaussian data and call them “normal”, in the sense of being the “norm”.

Hurst’s [109, **Figure 2**] shows that there is a linear relationship between $\log(\frac{R}{\sigma})$ and $\log(N)$ for all sets in which there are enough groups. The equations of these lines are (for $\mathbf{1.8} \lesssim \log(N) \lesssim \mathbf{3}$ [109, in **Figure 2**])

$$\log\left(\frac{R}{\sigma}\right) = K \log\left(\frac{N}{2}\right) = \log(R_\sigma). \quad (37)$$

R_σ is called the *rescaled range of fluctuations*, in this case, of the Nile [160]. The value of \mathbf{K} in Table 2 of Hurst [109] is positive and (calculated by me) **0.70 (0.69 – 0.72)** (median and 95% confidence interval, calculated according to Hodges and Lehmann [100]), a small dispersion, perhaps somewhat skewed upwards. It is clear from the figures that for each set of phenomena a straight line fits the data well, and the remarkable fact that \mathbf{K} , the slope of the line, varies little from one set to another. A summary of the mean of the K values obtained for the 690 separate values that Hurst computed, which is equivalent to $\approx \frac{\mathbf{1.3}}{\text{month}}$ of the values that Hurst measured during years in which he devoted himself to that. The fraction $\approx \frac{\mathbf{1.3}}{\text{month}}$ varies little, but *probably reflects what would be expected for a large river: whose changes are slow*. The number of data used $\approx \frac{\mathbf{1}}{\text{month}}$, is curious since some contemporary information suggests that the level of the Nile is measured daily [3].

So far we have followed as closely as we could the data from Hurst [109]. Here we must point out, however, that Eq. (37) can be rewritten in general form as

$$\log_b\left(\frac{R}{\sigma}\right) = \log_b(R_\sigma) = K_b \log_b\left(\frac{N}{2}\right), \quad (38)$$

which suggests that straight lines are obtained by logarithms of any base. From here on we will join most authors calling \mathbf{K}_b the **Hurst’s coefficient** and denote it as \mathbf{H} . An extremely important particular case is

$$\begin{aligned} \ln\left(\frac{R}{\sigma}\right) &= \ln(R_\sigma) = H \ln\left(\frac{N}{2}\right) \\ R &= \left(\frac{N\sigma}{2}\right) e^H \implies R_\sigma = \left(\frac{N}{2}\right) e^H \\ \therefore H &= \ln\left(\frac{2R}{N\sigma}\right) \quad \square \end{aligned} \quad (39)$$

If R is Gaussian with mean μ and variance σ^2 (that is $\mathcal{N}\{\mu, \sigma^2\}$, as assumed by Hurst), it may also be written

$$H = \ln\left(\frac{2}{\sigma N}\right) + \ln(\mathcal{N}\{\mu, \sigma^2\}), \quad (40)$$

so, even when R is Gaussian, H wont be.

Hurst [109, p. 19] considers the case where the annual water demand is less than the average river flow, but not less than the minimum annual flow recorded. In this case you have an approximate, B , equal to what is required and less than *the average*, M , and we need to know the largest *accumulated deficit*, S , which must be covered with stored water. This can be determined for any particular record of the cumulative deviation curve.

For **Figure 11**, $\mathbf{0} \rightarrow \mathbf{X}$ is the abscissa, which represents the value of the mean, with respect to which the other values of the figure are graphed. If we now produce an estimate B less than the average storage (axis $\mathbf{0} \rightarrow \mathbf{X}$) it will be increased each year in the magnitude $M - B$ above what was the estimated M . This can be determined from the original curve of cumulative deviations by drawing an axis $\mathbf{0} \rightarrow \mathbf{X}$ passing through the point F whose ordinate is $-\mathcal{N}(M - B)$. The curve ordinates referred to the **0axis** $\rightarrow \mathbf{X}_1$ show storage changes with water withdrawals B . Storage drops from P to Q , $P \rightarrow c + d \rightarrow Q$. This is the amount of storage S that would have been necessary to meet the demand B .

S was determined for various water demands for each of 38 types of phenomena such as the kinds of river discharges, rainfall, evaporation, use, and temperature that determines evaporation. The results for each class of events were grouped according to extraction, and the means of these groups were plotted. Evaporation was an important factor determining the salinization of Lake Nasser [6]. Two relationships fit to the results really well. The adjustment is (this strange equation is Hursy's *verbatim* [109, Eq. (3)]), although the interrogation sign is mine:

$$\log_{10}\left(\frac{S}{R}\right) = -0.08 - \overbrace{\mathbf{1.00}}^? \left(\frac{M - B}{\sigma}\right). \quad (41)$$

From there Hurst [109, Eq. (4)] somehow gets

$$\frac{S}{R} = 0.97 - 0.95\sqrt{\frac{M - B}{\sigma}}. \quad (42)$$

The average value of N from which these results are calculated is 96. It will be seen that in the adjustment, on the range of observations, there is no significant difference between one type of relationship and the other. If the figures are examined you will notice values of these kinds of phenomena are indistinguishable.

Hurst data on the Nile river is indeed priceless, but as seen in Eqs. (41) and (42), his algebra is sometimes strange. Another source of uncertainty in Hurst's data analysis is his unproven data Gaussianity, which is important to relate his exponent (now called H) with D , the fractal dimension of Nile's water level fluctuations [143, 70, 71, 200]. For me Hurst variable denomination is also strange and not easy to follow. All these peculiarities probably reflect Hurst's isolation, and also perhaps his decision of starting to write on his work late in his life.

5.3. Validity of the relationship between the Hurst's coefficient and its proposed relation with the fractal dimension.

The origin of the association between the two parameters was initially proposed by Mandelbrot and Wallis [146], with Mandelbrot's success in finding fractal systems in the most diverse places, seemed to be evidence for a relationship between the Hurst exponent and the fractal dimension, Φ , of two-dimensional systems was a simple relationship such as

$$D = 2 - H \quad (43)$$

[139, 94, 184, 185]. Thanks to Mandelbrot's success, fractal analysis has been applied to time series, profiles, and natural surfaces in almost every scientific discipline.

More recent analyses [143, 70, 71, 200] indicate that the relationship between fractal dimension and Hurst's coefficient is actually more complex than initially thought, and is not described by Eq. (43).

The trouble with Hurst's analysis is that he measured Nile River "levels" respect to some river bottom or "zero" which is not precise. By definition the Nile River level is never negative respect to this "zero". Because of this, the measurements in Figure 11 are done to are some mean level which is never zero, but is taken as "zero". And as indicated by my Eq. (39) (taken from Hurst work) H

Several authors have developed independent and (more?) exact methods to evaluate the Hurst coefficient [71, 68, 181] **which do not presuppose the Gaussianity of the data** that Hurst made and even consider the effect of the data 'pathological' distributed with Cauchy PDF [49, 169, 215, 219]. The discussion of "pathological distributions" like Cauchy's is neither trivial nor irrelevant. These distributions are not Gaussian, and have neither mean nor variance. The data that Hurst discusses are deviations from the level of the Nile from its mean, estimated \bar{x} , this is a random variable, whose mean is

$$\overline{\Delta x_i} = \frac{\sum_{i=1}^n (x_i - \bar{x})}{n} = 0 \quad (44)$$

and its apparent variance is

$$\text{var} [\overline{\Delta x_i}] = \frac{n+1}{n-1} \sum_{i=1}^n (x_i - \bar{x})^2. \quad (45)$$

If \mathbf{x}_i and R [see Eq. (35)] were Gaussian as assumed by Hurst, then $\overline{\Delta x_i}$ and R would have Cauchy PDF and *no operation with its apparent mean and/or apparent variance would make sense*. The Eqs. (44) and (45) can be calculated but are meaningless for a Cauchy distribution without central moments [79, 81, 82, 83, 207, 80]. If \mathbf{x}_i is not Gaussian the problem is similar, an unknown pathological random variable whose mean and variance estimated from a sample, are meaningless, because the pdf of count come has no mean or defined variance. *All sampling theory makes sense if and only if, the parameters that are estimated from the sample are approximations of the parameters of the population we sample.*

Recent evidence indicates that the relationship between the Hurst exponent and the fractal dimension is neither linear nor simple. *It does not seem justified to consider that the fractal dimension and the Hurst exponent are related to a simple linear relation*, so we will not devote more attention here.

6. Chaos, Strange Attractors, and Mathematics.

The idea that certain systems, numerically apparently very simple, could not have predictable values except at short times, was born when Lorenz [133] tried to solve a model of climate. The Lorenz model focused on three simultaneous equations (with slightly modified notation) which ate a numerical approximation to Rquation System (1):

$$\begin{aligned} x_{t+1} &= -\sigma x_t + \sigma y_t \\ y_{t+1} &= x_t z_t + \gamma x_t - y_t \\ z_{t+1} &= x_t y_t - b z_t \end{aligned} \quad (46)$$

where x_t , y_t and z_t represent the model variables in the iteration t , and σ . and γ are parameters set by the researcher before simulation (see [133] for details). In 1963 Lorenz used an analog computer where the variables of the simulated model were introduced by varying knobs that modified parameters of the simulator circuit. The analog circuit produced electrical signals that represented the results, these were printed, and before turning off the computer, Lorenz saved the values of the last set $\{x_{t+1}, y_{t+1}, z_{t+1}\}$ that he reintroduced into the system when he turned on the device the next time.

As long as the system operated without interruptions, the values stayed within a parallelepiped rectangle of sides $\{\mathbf{X}_{max}, \mathbf{Y}_{max}, \mathbf{Z}_{max}\}$ (a set of its solutions is

presented in **Figure ??**). The solution never passes through the same point twice, but evolves around that right parallelepiped forever. It seems as if something attracts the system to evolve there, thus the concept of *attractor* was coined to describe situations like this. Simply put, a attractor set \mathbf{A} for a dynamical system is a closed subset of phase space [206] such that “many” (most?) of the initial conditions the system evolves towards \mathbf{A} [152]. In the case of the Lorenz ensemble, the system solution never passes through the same place twice, a feature that coined the name *strange attractor*. In the Lorenz model the impossibility of reproducing or continuing from the point where it ended. This is due to the impossibility of introducing an earlier trajectory due to the imprecision of the controls of analogue systems. With digital computers, the researcher chooses an initial numerical value of his interest, this initial value is “type” always the same. At least on the same computer with the operating system and the accuracy of the processor it has, it is always handled the same and the initial (graphic) calculation is always the same. But, if the system stops and its variables are saved, behave the same as the analog Lorenz’s computer, the graph when rebooted does not follow the same trajectory: it becomes irreproducible: chaotic.

For nearly 20 years, Lorenz’s work received little attention. Only when strange attractors began to be observed in physics and then in almost every branch of science did Lorenz’s work became fundamental. Perhaps because of the shape of the Lorenz Attractor, the sensitivity to initial conditions in climate prediction was called the “butterfly effect”. Strange attractors appeared everywhere [15]. The mathematics behind strange attractors can be extremely simple as follows from the set of equations (46), but the implications deep.

6.1. Fractals and two-dimensional strange attractors.

As we have already said, the definition of fractal by Mandelbrot [139, 144] occurred almost 20 years after Lorenz’s work [133] and introduced interest in a class of, especially, two-dimensional strange attractors (see **Figure 12**). They were not really new, the sets of Julia [113] were published 60 years earlier. Just as the development of nonparametric statistics benefited from the emergence of computers after the 1940s, and their cheapening increased accessibility in the 1950s and cheapening with powerful and easily accessible microcomputers in the 1980s. As consequence, rapid advances occurred in processioning of iterative calculation and graphing. Thus systems that require iterative computation and graphing were developed. Such as systems, representing chaos, iterative and fractal systems such as the Julia sets [113, 136, 126] and the beautiful and fascinating Mandelbrot set. [138, 140, 141, 145, 144, 126].

The initial problem with fractal analysis was that physicists used it to study diverse systems where they determined the fractal dimension with the same precision

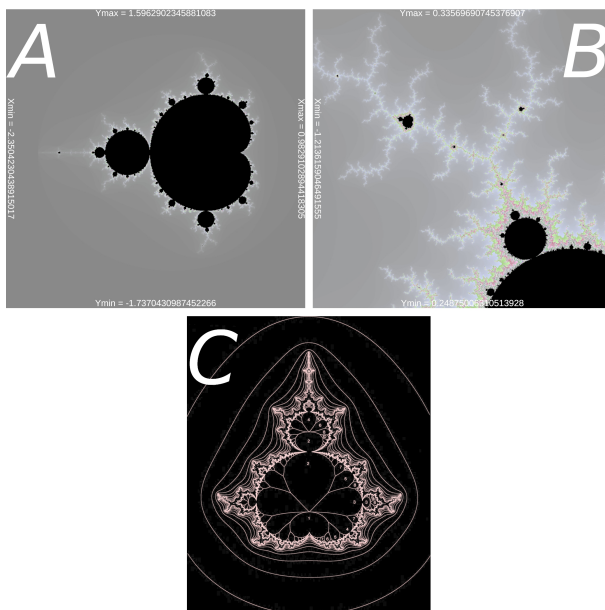


Figure 12: **Mandelbrot set: Calculation in relation to n .** **Panel A:** With initial values to display “all” the set. Panel A was calculated by taking up to $n = 1024$. Images calculated with JavaLab’s Java program, available at [5]. The scales indicated in **Panel A** are: $x_{max} = 0.98291028944183$, $x_{min} = 0.98291028944183$, $y_{max} = 1.59629023458811$ and $y_{min} = -1.73704309874523$. **Panel B** are: $x_{max} = -1.12666906030052$, $x_{min} = -1.21361590464915$, $y_{max} = 0.335656969074538$ and $y_{min} = 0.248750063105139$. The values of (x_{min}, x_{max}) and (y_{min}, y_{max}) , are the initial values of the calculation in each case: $Z_o = x_{min} + x_{min}i$ and $C = y_{min} + y_{max}i$. **Panel B:** Enlarged to show the appearance of structures similar to those in Panel A, as it is linearly expanded ≈ 38.4 times. **Panel C:** Based on Figure 34. by Mandelbrot [140]. In Panel C you can see some digits that are the $n = 1, \dots, 7$, of a mapping such as $Z_{n+1} \mapsto Z_n^2 + C$. The figure, which shows self-similarities when enlarging as black images in the branches of the whole. The scales are the coordinates of the graph.

with which other physical constants are studied.

6.2. The Mandelbrot set.

The Mandelbrot set [136, 140, 141, 33] the graphs shown in **Figure 12** is another example of an attractor as simple as Eq. (46) by Lorenz [133] which, however, hides a great conceptual depth.

Let’s look at some details about the Mandelbrot equation, it is an equation

that has solutions based on a variable $Z \in \mathbb{C}$ and a constant $C \in \mathbb{C}$, as follows:

$$\begin{aligned} Z_{n+1} &= \langle Z_n^2 + C \rangle \mid [(\mathbf{Z}_n = z_{n,re} + z_{n,im}\mathbf{i}) \wedge (C = c_{re} + c_{im}\mathbf{i})] \\ &\implies (Z_n \in C) \wedge (Z_{n+1} \in C) \wedge (C \in C) \end{aligned} \quad (47)$$

where $\mathbf{i} = \sqrt{-1}$. Eq. (47) is sometimes written [138] $Z_{n+1} \mapsto Z_n^2 + C$. With the *Zmapping* $\mapsto f(Z, C)$. Where $f \in \mathbb{R}$ is an *irrational function* (\mathbb{Q}) so that ($f(Z) \in \mathbb{Q}$) of Z and C , consider the iterated maps $Z_n = f(f(\dots f(Z_0)\dots))$ of the point Z_0 .

Square the complex numbers Z and C to create a new number Z . Square the new number Z and add C to produce another Z . Mandelbrot's set is another example of mathematical simplicity that hides a great depth of concepts. The Eq. (47). apart from including complex numbers, $Z \in \mathbb{C}$, can hardly be simpler, it only requires a square of a complex number

$$Z_n^2 = [(z_{re,n}^2 - z_{im,n}^2) + 2(z_{re,n}z_{im,n})\mathbf{i}] \quad (48)$$

Notice that there is a particular case where Z_n^2 becomes imaginary, this is

$$\begin{aligned} z_{re,n} = z_{im,n} &\implies Z_n^2 = 2(z_{re,n}z_{im,n})\mathbf{i} \\ \therefore \mathbf{Z}_n &= \mathbf{i}\sqrt{2z_{re,n}z_{im,n}} = \sqrt{2}z_{.n}\mathbf{i} \end{aligned} \quad (49)$$

The dot in $z_{.n}$ recognizes that both components are equal. But in general, if the situation foreseen in Eq. (49) holds, the next real component of Z_{n+1} depends entirely on the complex constant C :

$$\begin{aligned} Z_n^2 &= z_{re,n}^2 - z_{im,n}^2 + 2(z_{re,n}z_{im,n})\mathbf{i} \\ Z_{n+1}^2 &= z_{re,n}^2 - z_{im,n}^2 + 2(z_{re,n}z_{im,n})\mathbf{i} + c_{re} + c_{im}\mathbf{i} \\ \dots &= [z_{re,n}^2 - z_{im,n}^2 + c_{re}] + [2(z_{re,n}z_{im,n}) + c_{im}]\mathbf{i} \quad \cdot \quad (50) \\ \therefore \mathbf{Z}_{n+1} &= \sqrt{[z_{re,n}^2 - z_{im,n}^2 + c_{re}] + [2z_{re,n}z_{im,n} + c_{im}]\mathbf{i}} \quad \square. \end{aligned}$$

Repeat this \aleph_0 times [33, 5, 11]⁸. A graph, co, or those presented here in **Panel 12A** is the solution ‘‘complete’’ and ‘continuous’ of the Eq. (47) and the **Panel 12B** is a ‘‘window’’ of a solution which extends $\approx \times 40$ iterations [33, 5, 11].

⁸ \aleph_0 is an infinitely large cardinal number

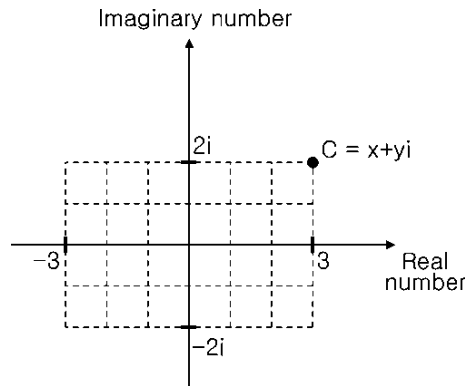


Figure 13: **Mandelbrot set. Determination of C .** A window defined for complex numbers (x, yi) with C defined in the upper right corner. Figure based on another of [5].

6.2.1. How to calculate the Mandelbrot set.

Mandelbrot found that the value of Z continued to increase or oscillate between two small values “depending on C ” [5]. He used a computer to calculate each value of C and plotted it on the screen as a not “radial” dot Z . The result is somewhat difficult to describe, a purely generic structuring process (squares, triangles, circles), each Mandelbrot graph is the solution of Eq. (47) up to $n + 1 \rightarrow \aleph_0$. The resulting graph is called the Mandelbrot set. Mandelbrot continued to magnify the image, but the same structures continued to appear (self-likeness). No matter when he left, for $n + 1 \rightarrow \aleph_n$, the same images continued to appear.

The procedure can be described as: create a window with complex coordinates (x, yi) with one pixel per computer screen number and call it $C = x, yi$, the others are possible values of $Z_{n+1} \mapsto Z_n^2 + C$ defined in Eq. (47). Usually, the range of the x axis goes between $(-3 \leftrightarrow +3)$, and the range of y values goes between $(-2 \leftrightarrow +2)i$. In this range, you can see the entire picture of the Mandelbrot set. *if the values of Z do not diverge is represented on site with a black dot on the screen*, the result is a Mandelbrot set. Usually if $n > (2 \leftrightarrow 4)$ this is greater than, it is recorded as a divergence and the recurring relationship is stopped.

The more the recurring relationship is repeated, the more detailed we can get a figure. However, this cannot be calculated indefinitely. Due to limitations of computing power, even if high-precision real numbers such as those indicated in **Figure 12** are used, therefore the process stops when it reaches a reasonable precision: $n = 1024$ in the **Figures 12A** and **B**, or $n = 16$ in the **Figure 14**.

There is an aesthetic aspect to fractal images. An artistic look can be added to graphics by adding arbitrary colors to successive Z_n values. This is done, sometimes

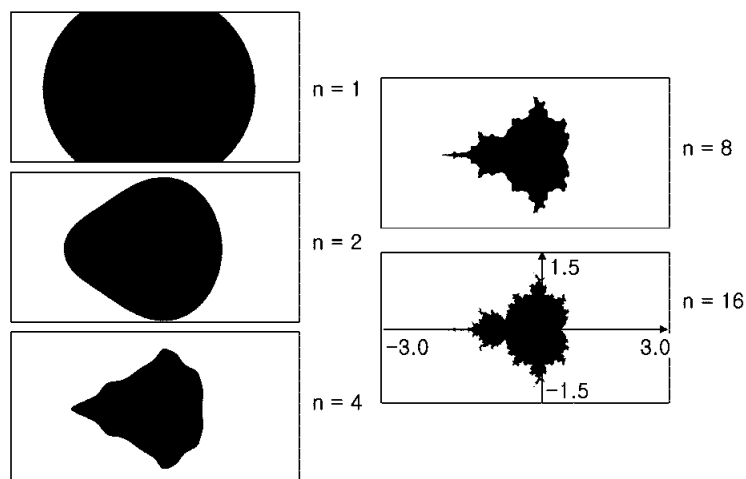


Figure 14: A window defined for complex numbers $(x, y\bar{i})$ with C defined in the upper right corner. Figure based on another of n the number of iterations. Figure based on [5]

associating color regions to ranges of values of n , where usually the use of black for $n \leq 7$ is maintained, and then other color bands to the liking of the calculator. One of many examples are our **Figures 12A, B and C** The graphics using the Mandelbrot set have become an element to show aesthetics and computing power accompanied by the sets of Julia [178].

Some details of the calculation and graphing of the Mandelbrot set have been extended here to describe in part the information contained in the Mandelbrot set, the fruit of human ingenuity and the simple mathematics that underlies it.

7. Use and abuse of the fractal dimension.

The introduction of the concept of chaos in climate by Lorenz [133, 132, 161], from where, after a delay, it invaded the rest of science widely, and the introduction of the concept of fractal by Mandelbrot [139, pg. 15 and Ch. 39] changed the view of the science of numerous systems, as it emerges, partially, from the previous discussion. His problem: the same as data analysis and statistics: mathematics.

7.1. Misuse of the fractal dimension estimation methods.

A fundamental problem in fractal analysis is using a poor method or not understanding the limitations of the method being used. In this paper we have presented Mandelbrot's original definition of the concept of fractal dimension.

According to Mandelbrot [139, pg. 15 and Chap. 39]

“A fractal is by definition a set for which the Hausdorff-Besicovitch dimension strictly exceeds the topological dimension. Every set with a non integer D is a fractal.”

The definition has a problem, however, since it depends on estimating the Hausdorff-Besicovitch dimension of the interest function.

Although Hausdorff-Besicovitch definition is simple:

$$D_{HB} = -\lim_{\epsilon \rightarrow 0} \frac{\ln[N(\epsilon)]}{\ln(\epsilon)} = -\lim_{\epsilon \rightarrow 0} \log_{\epsilon}[N(\epsilon)]$$

the definition implies that $N(\epsilon) \rightarrow \infty$, a number that, however large, in most experimental cases is not available.

In the definition of $N(\epsilon) \implies N(\epsilon) \in \mathbb{R}$ a very large real number, $\approx \infty$, but this may not seem true in waveforms sampled in discrete mode.

A second interpretation may be that $\{N_i(\epsilon)\}$ represents a set of size N such that

$$N_i(\epsilon) \mapsto \begin{cases} i \in \{1 \leftrightarrow \aleph_0\} \implies N_i(\epsilon) \in \mathbb{R} \\ i \in \{1 \leftrightarrow \infty\} \implies N_i(\epsilon) \in \mathbb{R} \end{cases}, \quad (51)$$

but this may not be true, in the case of, for example, the decimal digits of π : $N_i(\epsilon) \in \{0, 1, \dots, 9\}$ [186]. In such cases, D_{HB} may be undefined, or greater, than the value of D for $\{\log_{\epsilon}[N(\epsilon) \rightarrow \aleph_0]\}$. Under these condition Sevcik's D_S , or any empirical estimate of D_{HB} will be partially uncertain. In Eq. (51), \aleph_0 is the largest value of i which is ($i \in \mathbb{Z}$), the set of all integer numbers. Minimizing that uncertainty is represented by a very large set of numbers. If $\aleph_0 \rightarrow \infty$ the uncertainty of the decimal of π will be represented by real numbers [186]

7.2. Accurate ways to measure D .

The most accurate (for even $n > 2$ dimensional spaces) ways to determine D were introduced by physicists [156, 207, 79, 81, 83, 156, 80]. This often involves studying the same system in Euclidean spaces of different dimensions, using Lyapunov exponents [10], and demands the use of complicated mathematics.

7.2.1. Baseless relation between fractal dimension and the Hurst's coefficient (H).

In the early days of the definition and “extension” of the concept of fractal, Mandelbrot [139] was liberal. The association between the Hurst exponent and the fractal dimension that we discuss in this here, we find an example.

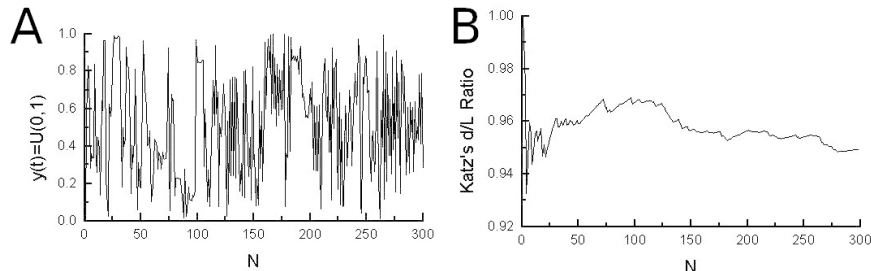


Figure 15: **Properties of the ratio d/L for a curve generated with Monte Carlo simulation [52]. Panel A:** Shows a waveform constructed by joining with straight lines a series of uniform pseudo random numbers in the interval $(0,1)$. **Panel B:** Ratio d/L calculated for the corresponding point of the abscissa in the top panel. In both panels the abscissa is N . other details in the original publication [184, 185, Figure 2] and in the text of the this paper.

7.3. Katz “fractal dimension” does not measures fractal dimension.

Figure 15B shows that d/L oscillates a lot at first, but then stabilizes with $N \geq 50$. This confirms the uselessness of [Eq. (4)] to determine the fractal dimension of a curve. This is true for all waves for which d/L is asymptotically constant after sampling $m < \infty$ points for $N' < \infty$ Eq. (52) also implies that the values of D_K is arbitrarily determined by the choice of N . The boundary condition, $N' \rightarrow \infty$, can be made if t_{max} (the sampling duration) remains constant but the sampling interval $\delta \rightarrow 0$. I submitted Eq.(52) in the first version of my papr [184, 185] to the journal whee Katz paper appeared and was rejected, more than 10 years later the published a Letter to The Editor with an “experimental proof” suggesting that there is “something wrong” with D_K [42]. In spite of all this D_K is still used by authors with ignorance of algebra, usally because they know nothing else and they found it ‘pretty’ [61, 66, 63? , 67, 173, 74, 73, 39, 162, 176, 177, 134, 88, 69].

Katz [116] Eq. (4) is wrong [184, 185] This becomes apparent if we calculate the following limit:

$$\lim_{N' \rightarrow \aleph_0} D_K = \lim_{N' \rightarrow \aleph_0} \left[\frac{\log(N')}{\log(N') + \log(d/L)} \right] = 1 \quad \square. \quad (52)$$

In the original version [184, 185] the limit is made up to ∞ , but since $N' \in \mathbb{Z}$, it seems here more rigorous to do it up to \aleph_0 . The limit in Eq. (52) shows that Eq. (4) predicts that all curves are analyzed with the Eq. (4) as the discretization is improved by making N' very large or \aleph_0 , we will discover that all curves are straight lines with $D_K = 1$. It could be argued that the limit in Eq. (52) has been derived assuming that d/L is a constant. This is discussed in [184, 185] with the analysis of data produced with Monte Carlo simulation [52] as shown in Figure 15.

Also a ‘liberal’ idea of Mandelbrot [139] was associating complex systems with the fractal dimension. An example of this was its association of the length of a river with a straight line distance between its source and its mouth. This view inspired the fractal dimension estimated with Katz’s method [116]:

$$D_K = \frac{\log(N')}{\log(N') + \log(d/L)}.$$

This definition of Katz has a problem: **only applies to short waveforms** and in no case converges to Φ . This is easy to see considering the limit in Eq.(52) [184, 185].

7.4. Sevcik’s fractal dimension.

Given the inability of D_K to predict Φ , another method was developed to calculate the fractal dimension [184, 185], this method describes what is now called Sevcik’s fractal dimension in GogScholar [4] refers 200 (October 2024) citations of the use of Sevcik’s fractal dimension [184, 185], using this algorithm. The [184, 185] algorithm is a double linear transformation [Eqs. (8) – (15)].

As said D_S is calculated in a linear transformation of the space where the waveform exist, thus both spaces have the same metric properties, which includes D_{HB} , Φ and D_S [20, 184, 185] **if $N \rightarrow \infty$** . Since the topology of a metric space does not change under a linear transformation, it is convenient to transform a wave into another normalized space, where all axes are equal. I proposed the use of two linear transformations that map the original wave function into another embedded in an equivalent metric space [please see [20] for a very readable discussion of metric spaces]. In recent years, this way of calculating the fractal dimension of a wave has been called the Sevcik fractal dimension [179], which here we call D_S . This determines that the original function and is transformed into anther into a space with equal coordinates and with units. **Thus it is not surprising that, as shown in Subs-subsection 3.2.2, D_S converges to Φ as $N \rightarrow \infty$.**

Slil if

$$N \rightarrow \begin{cases} \aleph \in \mathbb{Z} \\ \infty \in \mathbb{R} \end{cases},$$

N is **VERY** large, and nobody works that much,so, for any real life estimate of D_S we will have $D_S < \Phi$. If we are interested in the decimal sequence of π [186], we can compare this sequence, $\{i_{\pi,i}\}_{i=1,2,\dots,k,\dots N} = \{i_{\pi,1}, i_{\pi,2}, \dots, i_{\pi,k}, \dots, i_{\pi,N}\} \wedge [i_{\pi,k} \in \{0, 1, 2, 3, 4, 5, 6, 7, 8, 9\}] \in \mathbb{Z}$. If the decimal sequence of π is bob periodic and all digits are equally likely, they must be distributed as a random uniform variable [86] set where the probability of any digit in the set $\{0, 1, 2, 3, 4, 5, 6, 7, 8, 9\}$ has a probability of $\frac{1}{10}$,i.e., with a “reasonable” N : a sort of white noise [94]. A real white nose is shown in Figure 8A, where the points are all Gaussian real numbers.

As of July 2024, π has been calculated to $2.02 \cdot 10^{14}$ digits [13], and 10^9 are easy to generate on a personal computer [23, 186]. Thus many sequences of series of random uniformly distributed each with a probability $\frac{1}{10}$ decimal digits N and compared with the same numbers of π of decimals [186]. The same procedure may be used to compare an observed series and compare it with a random sequence of known properties.

7.5. Avoiding intuitive conclusions in relation with Φ .

Although it is possible to prove for fractal functions such as Koch snowflake [211, 184, 185] that $\lim_{N \rightarrow \infty} D_S = D_{HB}$, for more complex functions this can be difficult [184, 185, 186, 179] and a demonstration may not be easy and require *reliable* Monte Carlo simulations [192, 153, 184, 185, 186, 179].

Intuitive estimations of Φ are dangerous. Even a solid mathematician as Mandelbrot devised more or less intuitive estimates for rivers using the length of the river and the straight line distance between the river fountain to the river end [139], the Katz D_K fractal dimension is a generalization Mandelbrot's river Ψ . Even if the fractal dimension defined by Mandelbrot is the ratio of two "natural" river, perhaps better for long rivers, but D_K gets worse as the number of discretized waveform points grows [116, 184, 185].

8. Pitfalls using the fractal concept.

8.1. The use of the term 'fractal' to promote unscientific theories.

The term fractal is sometimes used as a manner to provide a 'deep scientific' meaning, to propositions lacking any scientific sport. This seems the case this seems the case of a theory unifying gravity and quantum physics [148, 149, among several YouTube videos and a LinkedIn communication] or with fancy sounding theories to synthesize drugs [14].

8.2. Cautions when using fractal dimension estimates.

Authors make mistakes and reviewers not always understand the concept of fractal dimension. Between the non physicists, fractal analysis became fashionable in this century. Unfortunately, too many authors (and their reviewers in journals) do not pay attention to the mathematics of the fractal analysis methods, thus the Katz and Higuchi methods have gained undue popularity, specially in medical, psychological, psychiatric and low level technique papers, there are too many examples to cite them precisely here but many examples can be found with GoogleScholar (<https://scholar.google.com>) or with sites such as

Academia.edu (<https://www.academia.edu>) (among other scientific paper browsers) intermixed with valuable papers.

Another problem is (excuse the neologism) that we will call: the “curve nicety”: a principle that demands that, above any other principle, the curves and data that we enter in a work must look ‘pretty’. Of course, if they are also true better than better. While Eq. (52) [184, 42, 185] demonstrates beyond doubt that the called “fractal dimension of Katz” [116] is different from 1 only if the starting points of any waveform are considered and is equal to 1 for any waveform other than a straight line when $N \rightarrow \aleph_0$ or $N \rightarrow \infty$ and $\lim_{N \rightarrow \infty} D_{HB} \neq 1.0$. The problem is that Eq. (4) does not have an “optimal” to estimate D_K Eq. (52), *always underestimates* Φ even if you underestimate it more with large N . However a number of authors base their choice of a method of assigning fractal dimension to their curves choose the one that makes their data look “prettier” and thus preserve meaningless methods [61, 66, 63? , 67, 173, 74, 73, 39, 162, 176, 177, 134, 88, 69, 2, 56, 218, 198, 199, 92, 1, 50, 127, 128, 187, 8].

Acknowledgments.

Free open source software used.

This manuscript was written in L^AT_EX (T_EXLive 2023, <https://www.tug.org/texlive/>).Tex using *T_EXstudio* 4.8.4 (<https://www.texstudio.org>)for Linux, an open source free L^AT_EX editor. All the silverware used here ran under Cinnamon Linux Mint 22 “Wilma” (<https://www.linuxmint.com/download.php>).

Figures reproduced from the literature.

Figure 11 of this work is the reproduction of the **Figure 1** of the work [110] published on line by *Ministry of Public Works*, Egypt on January 04, 2010 [110] of work [107].

The article is provided under license from Taylor & Francis which the work states as follows:

This article may be used for research, teaching, and private study purposes. Any substantial or systematic reproduction, redistribution, reselling, loan, sub-licensing, systematic supply, or distribution in any form to anyone is expressly forbidden. Terms & Conditions of access and use can be found at <http://www.tandfonline.com/page/terms-and-conditions>.⁹

⁹Internet access reproduced here exactly from the original.

References

- [1] A. H. Al-nuaimi, E. Jammeh, E. L. Sun, and Ifeachor. Higuchi fractal dimension of the electroencephalogram as a biomarker for early detection of Alzheimer’s disease. In 2017 39th Annual International Conference of the IEEE Engineering in Medicine and Biology Society (EMBC), pages 2320–2324. IEEE Engineering in Medicine and Biology Society, 2017. doi: 10.1109/EMBC.2017.8037320.
- [2] A. Anier, T. Lipping, S. Melto, and S. Hovilehto. Higuchi fractal dimension and spectral entropy as measures of depth of sedation in intensive care unit. In The 26th Annual International Conference of the IEEE Engineering in Medicine and Biology Society, pages 526–529, San Francisco, CA, USA, Sep 1–5 2004. IEEE Engineering in Medicine and Biology Society. doi: 10.1109/IEMBS.2004.1403210.
- [3] Anonymous. A river that decides tax rates. YpuYube, May 22 2015. URL https://www.youtube.com/watch?v=oqjYrUJo_SM.
- [4] Anonymous. Google scholar, Retrieved: November 9 2020. URL <https://scholar.google.com/citations?hl=en&user=0VhfpTIAAAAJ>.
- [5] Anonymous. Mandelbrot set. Fractal simulation. JavaLab, Jan 15 2020. URL https://javalab.org/en/mandelbrot_set_en/.
- [6] Anonymous. Lake Nasser Mysterious : The Secret of lake 2021 Latest science documentary. YouTube, Science Tech Docs, Feb 18 2021. URL <https://www.youtube.com/watch?v=QKqRUX0xuls>.
- [7] Anonymous. Cantor set. WikipediA, The Free Encyclopedia, Apr 27 2022. URL https://en.wikipedia.org/wiki/Cantor_set.
- [8] Anonymous. Higuchi dimension. WikipediA, The Free Encyclopedia, Apr 23 2022. URL https://en.wikipedia.org/wiki/Higuchi_dimension.
- [9] Anonymous. List of fractals by Hausdorff dimension. WikipediA, The Free Encyclopedia, Apr 5 2022. URL https://en.wikipedia.org/wiki/List_of_fractals_by_Hausdorff_dimension.
- [10] Anonymous. Lyapunov exponent. WikipediA, The Free Encyclopedia, Jul 7 2022. URL https://en.wikipedia.org/wiki/Lyapunov_exponent.

- [11] Anonymous. Mandelbrot set. WikipediA, The Free Encyclopedia, Jun 24 2022. URL https://en.wikipedia.org/wiki/Mandelbrot_set.
- [12] Anonymous. Pi. WikipediA, The Free Encyclopedia, Jun 24 2024.
- [13] Anonymous. Chronology of computation of π . WikipediA, The Free Encyclopedia, Aug 24 2024. URL https://en.wikipedia.org/wiki/Chronology_of_computation_of_\pi.
- [14] Anonymous. Quantum Wonders: Redefining the Laws of Physics. YouTube, Skywise Cloud, Jan 25 2024. URL <https://www.youtube.com/watch?v=J9PAqg-nN8g>.
- [15] D. V. Anosov. Strange attractor. Encyclopedia of Mathematics, Aug 14 2014. URL https://encyclopediaofmath.org/wiki/Strange_attractor.
- [16] R. Badii and A. Politi. Statistical description of chaotic attractors: The dimension function. J. Stat. Physics, 40:725–750, 1985. doi: 10.1007/BF01009897.
- [17] D. H. Bailey and R. E. Crandall. On the random character of fundamental constant expansions. Exper. Mathem., 10:175–190, 2001.
- [18] D. H. Bailey and R. E. Crandall. Random generators and normal numbers. Exp. Math., 11:527–545, 2002.
- [19] D. H. Bailey, J. M. Borwein, C. S. Calude, M. J. Dinneen, M. Dumitrescu, and A. Yee. An empirical approach to the normality of π . Exper. Mathem., 21:375–384, 2012.
- [20] M. F. Barnsley. Fractals Everywhere. Academic Press Professional, Cabridge, MA USA, 1993.
- [21] C. Batista, G. D’Suze, F. Gómez, F. Zamudio, C. Sevcik, and L. D. Possani. Proteomic analysis of *Tityus discrepans* scorpion venom and amino acid sequence of novel toxins. Proteomics, 6:3718–3727, 2006. doi: 10.1002/pmic.200500525.
- [22] V. Becher and S. Figueira. An example of a computable absolutely normal number. Theor. Comp. Sci., 270:947–958, 2002.

- [23] F. Bellard. Computation of 2700 billion decimal digits of Pi using a desktop computer. bellard.org, Feb 2010. URL <https://bellard.org/pi/pi2700e9/pipcrecord.pdf>.
- [24] B. P. Belousov. Periodically acting reaction and its mechanism (All in Russian). Collection of abstracts on radiation medicine, 147:145, 1959.
- [25] J. S. Bendat and A. C. Piersol. Random data. Analysis and measurements procedures. John Wiley & Sons, New York, 2 edition, 1985.
- [26] M. Berry. Chaos and the semiclassical limit of quantum mechanics (is the moon there when somebody looks?). Quantum Mechan.: Sci. Persp. Divine Action, 41:56, 2001. URL <https://michaelberryphysics.files.wordpress.com/2013/07/berry337.pdf>.
- [27] A. S. Besicovitch. On linear sets of points of fractional dimensions. Math. Annalen, 101:161–193, 1929.
- [28] R. B. Blackman and J. W. Tukey. The Measurement of Power Spectra from the Point of View of Communications Engineering. Dover Publications Inc., New York, U.S.A., 1959.
- [29] L. Boltzmann. Lectures on gas theory. University of California Press–Dover, Berlely–New York, 1964.
- [30] E. Borel. Les probabilités dénombrables et leurs applications arithmétiques. Rend. Circ. Mat. Palermo, 27:247–271, 1909.
- [31] G. E. P. Box and M. E. Muller. A note on the generation of random normal deviates. Ann. Math. Stat., 22:610–611, 1958. doi: 10.1214/aoms/1177706645.
- [32] J. F. Bozeman III, R. Bozeman, and T. L. Theis. Overcoming climate change adaptation barriers: A study on food–energy–water impacts of the average American diet by demographic group. J. Ind. Ecol., pages 1–17, 2019. doi: 10.1111/jiec.12859.
- [33] B. Branner, J. Harrison, and P. J. Holmes. The Mandelbrot Set. In R. L. Devaney and L. Keen, editors, Chaos and Fractals The Mathematics Behind the Computer Graphics, volume Proceedings of Symposia in Applied Mathematics, ol 48, pages 75–105, Providence, Rhode Island, 1989. American Mathematical Society, publisher.

- [34] G. W. Brown and J. W. Tukey. Some distributions of sample means. Ann. Math. Statist., 17:1–12, 1946. doi: 10.1214/aoms/1177731017.
- [35] R. Brown. XXVII. a brief account of microscopical observations made in the months of June, July and August 1827, on the particles contained in the pollen of plants; and on the general existence of active molecules in organic and inorganic bodies. Phil. Mag., 4:161–173, 1828. doi: 10.1080/14786442808674769.
- [36] R. Brown. XXIV. additional remarks on active molecules. Phil. Mag., 6: 161–166, 1829. doi: 10.1080/14786442908675115.
- [37] L. F. Burlaga and L. W. Klein. Fractal structure of the interplanetary magnetic field. J. Geophys. Res.: Space Phys., volume:347–350, Jan 1 1986. doi: 10.1029/JA091iA01p00347.
- [38] S. D. Burt and D. A. Mansfield. The great storm of 15-16 october 1987. Weather, 43:90–110, 1988. doi: 10.1002/j.1477-8696.1988.tb03885.x.
- [39] C-Goh, B. Hamadicharef, G. T. Henderson, and E. C. Ifeachor. Comparison of Fractal Dimension Algorithms for the Computation of EEG Biomarkers for Dementia. In SPMC - Signal Processing and Multimedia Communications research group, pages 464–471, Professor José Manuel Fonseca, UNINOVA, Portugal, Jun 2005, Lisbon, Portugal, 2005. CIMED2005 Proceedings, IEE. URL https://www.researchgate.net/publication/40902603_Comparison_of_Fractal_Dimension_Algorithms_for_the_Computation_of_EEG_Biomarkers_for_Dementia.
- [40] G. Cantor. De la puissance des ensembles parfaits de points. Acta Math., 4: 381–392, 1884.
- [41] M. Cao, Q. Ren, and L. W. Y. Luo. Length fractal dimension algorithm picks up the first arrival of seismic waves. Petrol. Geophys. Prosp., pages 509–514, 2004.
- [42] P. Castiglioni. Letter to editor: What is wrong in Katz’s method? Comments on: “A note on fractal dimensions of biomedical waveforms”, 2010.
- [43] G. J. Chaitin. On the simplicity and speed of programs for computing infinite sets of natural numbers. J. ACM, 16:407–422, 1969.
- [44] G. J. Chaitin. Algorithmic entropy of sets. Comp. Math. Appl., 2:233–245, 1976.

- [45] G. J. Chaitin. Algorithmic information theory. Cambridge U. Press, Cambridge, 1987.
- [46] D.-R. Chen, R.-F. Chang, C.-J. Chen, M.-F. Ho, S.-J. Kuo, S.-T. Chen, S.-J. Hung, and W. K. Moon. Classification of breast ultrasound images using fractal feature. J. Clini. Imag., 29:235–245, 2005r. doi: 10.1016/j.clinimag.2004.11.024.
- [47] D. V. Chudnovsky and G. V. Chudnovsky. Approximations and complex multiplication according to Ramanujan. In L. Berggren, J. Borwein, and P. Borwein, editors, Pi: A Source Book, chapter 63, pages 596–622. Springer-Verlag, New York, 2nd edition, 2000.
- [48] D. Colquhoun. Lectures on Biostatistics. Clarendon Press, Oxford, 1971.
- [49] H. Cramér. Mathematical Methods of Statistics. Princeton, 18th edition, 1991.
- [50] M. Cukic, D. Pokrajac, M. Stokic, s. Simic, V. Radivojevic, and M. Ljubisavljevic. EEG machine learning with higuchi fractal dimension and sample entropy as features for successful detection of depression. www.arXiv.org, Cornell University, May 15 2018. URL <https://arxiv.org/pdf/1803.05985.pdf>.
- [51] K. M. Cuomo and A. V. Oppenheim. Circuit implementation of synchronized chaos with applications to communications. Phys. Rev. Lett., 71:65–68, 1993.
- [52] G. Dahlquist and Å. Björk. Numerical Methods. Prentice Hall Inc., Englewood Cliffs, 1974.
- [53] M. Danos. Fractals and Chaos in Geology and Geophysics. Cambridge University Press, Cambridge, UK, 2 edition, Oct 19 2006. doi: 10.1029/98EO00263.
- [54] X. Diao, Q. Dong, Z. Yang, and Y. Li. Double-threshold cooperative spectrum sensing algorithm based on Sevcik fractal dimension. Algorithms, 10:96, Aug 21 2017. doi: 10.3390/a10030096.
- [55] O. Dovgoshey, O. Martio, V. Ryazanov, and M. Vuorinen. The cantor function. Expo. Math., 24:1–37, 2006. doi: 10.1016/j.exmath.2005.05.002.
- [56] T. L. A. Doyle, E. L. Dugan, B. Humphries, and R. U. Newton. Discriminating between elderly and young using a fractal dimension analysis of centre of pressure. Int. J. Med. Sci., 1:11–20, 2004. doi: 10.7150/ijms.1.11.

- [57] G. D'Suze and C. Sevcik. Scorpion venom complexity fractal analysis. Its relevance for comparing venoms. J. Theoret. Biol., 267:405–416, 2010. doi: 10.1016/j.jtbi.2010.09.009.
- [58] G. D'Suze, A. Rosales, V. Salazar, and C. S. C. Temas Seleccionados de Toxinas con Implicaciones BIOMÉDICAS y Métodos para su Estudio, chapter Identificación de Toxinas con Actividad Antineoplásica en el Veneno del Escorpión *Tityus discrepans*, pages 10–27. Red CYTED 212RT0467 Biotox, address, 2012. URL <https://www.iq.usp.br/biotox/images/stories/e-book.pdf>.
- [59] G. D'Suze, C. Castillo, C. Sevcik, J. Brazón, and C. Malavé. Scorpionism and dangerous species of Venezuela. In P. Gopalakrishnakone, L. D. Possani, E. F. Schwartz, and R. C. Rodríguez de la Vega, editors, Scorpion Venoms, volume 4 of Toxinology, pages 273 – 298. Springer, Dordrech, Germany, 2015. URL https://www.researchgate.net/profile/Carlos-Sevcik/publication/275893778_Scorpion_Venoms/links/5688657608ae1e63f1f7404d/Scorpion-Venoms.pdf.
- [60] G. D'Suze, M. Sandoval, and C. Sevcik. Characterizing *Tityus discrepans* scorpion venom from a fractal perspective: Venom complexity, effects of captivity, sexual dimorphism, differences among species. Toxicon, 108:62–72, 2015. doi: 10.1016/j.toxicon.2015.09.034.
- [61] B. Dubuc, J. E. Quiniou, C. Roques-Carmes, C. Tricot, and S. M. Zucker. Evaluating the fractal dimension of profiles. Phys. Rev. A, 39:1500–1512, 1989. doi: 10.1103/PhysRevA.39.1500.
- [62] J. Dunne. Storm hits home of 1987 'blunder weather forecaster' Michael Fish. The Standard, January 31 2013. URL <http://tinyurl.com/mr2b9a5n>.
- [63] A. Eblen-Zajjur and R. S. H. Vanegas. Fractal analysis of spinal nociceptive neuronal responses to receptive field stimulation and to heterotopic noxious stimulation in the rat. Neurosc. Res. Comm., 25:51–60, 1999. doi: 10.1002/(SICI)1520-6769(199907/08)25:1<51::AID-NRC6>3.0.CO;2-J.
- [64] B. Efron. The Jackknife, the Bootstrap and Other Resampling Plans. Society for Industrial and Applied Mathematics, Philadelphia, 1983.
- [65] T. Elbert, W. J. Ray, K. Z. J., J. E. Skinner, K. K. E. Graf, and N. Birbaumer. Chaos and physiology: Deterministic chaos in excitable cell assemblies. Phys. Rev., 74:1–47, 1994. doi: 10.1152/physrev.1994.74.1.1.

- [66] M. J. Embrechts and Y. Danon. Determining the fractal dimension of a time series with a neural net. In Intell. Engineering systems through artificial neural networks, volume 3, pages 897–902. Citeseer, 1993. URL <https://homepages.rpi.edu/~danony/Papers/Determining%20the%20Fractal%20Dimension%20of%20a%20Time%20Series.pdf>.
- [67] R. Esteller, G. Vachtsevanos, J. Echauz, and B. Litt. A comparison of waveform fractal dimension algorithms. IEEE Trans. Circ. Syst. I: Fund. Theor. App., 48:177–183, 2001. doi: 10.1109/81.904882.
- [68] M. Fernández-Martínez, J. T. S. M.A. Sánchez-Granero and, and I. Román-Sánchez. An accurate algorithm to calculate the hurst exponent of self-similar processes. Physics Letters A, 378:2355–2362, 2014. doi: 10.1016/j.physleta.2014.06.018.
- [69] A. Gil, V. Glavan, A. Wawrzaszek, R. Modzelewska, and L. Tomasik. Katz fractal dimension of geoelectric field during severe geomagnetic storms. Entropy, 23:On Line 1531, Nov 18 2021.
- [70] T. Gneiting and M. Schlather. Stochastic models that separate fractal dimension and the Hurst effect. SIAM review, 46:269–282, 2004. doi: 10.1137/S0036144501394387.
- [71] T. Gneiting and M. Schlather. Stochastic models which separate fractal dimension and hurst effect. www.arXiv.org, Cornell University, 2011. URL <https://arxiv.org/pdf/physics/0109031.pdf>.
- [72] T. Gneiting, H. Ševčíková, and D. B. Percival. Estimators of fractal dimension: Assessing the roughness of time series and spatial data. Stat. Sci., 27:247–277, 2012. doi: 10.1214/11-STS370.
- [73] J. Gnitecki and Z. Moussavi. The fractality of lung sounds: A comparison of three waveform fractal dimension algorithms. Chaos Sol. Frac., 26:1065–1072, 2005. doi: 10.1016/j.chaos.2005.02.018.
- [74] J. Gnitecki, Z. Moussavi, and H. Pasterkamp. Classification of lung sounds during bronchial provocation using waveform fractal dimensions. In The 26th Annual International Conference of the IEEE Engineering in Medicine and Biology Society, volume 2, pages 3844–3847. IEEE, 2004. doi: 10.1109/IEMBS.2004.1404076.
- [75] A. L. Goldberger. Is the normal heartbeat chaotic or homeostatic? Physiology, 6:87–91, 1991. doi: 10.1152/physiologyonline.1991.6.2.87.

- [76] M. A. González-Sponga, G. D'Suze, and C. Sevcik. Venezuelan arachnids. two new species of the *Tityus* genus (Scorpionida: Buthidae) and the chromatographic profile of their venom. J. Ven. Anim. Tox. Trop. Dise., 7:219–239, 2001. doi: 10.1590/S0104-79302001000200007.
- [77] M. Gorman, P. J. Widmannand, and K. A. Robbins. Nonlinear dynamics of a convection loop: A quantitative comparison of experiment with theory. Physica D, 19:255–267, 1986. doi: 10.1016/0167-2789(86)90022-9.
- [78] K. Gotoh, M. Hayakawa, and N. Smirnova. Fractal analysis of the ULF geomagnetic data obtained at Izu peninsula, Japan in relation to the nearby earthquake swarm of June–August 2000,. Nat. Hazards Earth Syst. Sci., 3: 229–236, 2003. doi: 10.5194/nhess-3-229-2003,2003.
- [79] P. Grassberger. On the Hausdorff dimension of fractal attractors. J. Stat. Phys., 26:173–179, 1981r. doi: 10.1007/BF01106792.
- [80] P. Grassberger and I. Procaccia. Measuring the strangeness of strange attractors. In The Theory of Chaotic Attractors, pages 170–189. Springer, 2004. doi: 10.1007/978-0-387-21830-4_12.
- [81] P. Grassberger and J. Procaccia. Estimation of the Kolmogorov entropy from a chaotic signal. Phys.Rev. A, 28:2591–2593, 1983. doi: 10.1103/physreva.28.2591.
- [82] P. Grassberger and J. Procaccia. Measuring strangeness of strange attractors. Phys. Lett. D, 9:189–208, 1983. doi: 10.1016/0167-2789(83)90298-1.
- [83] P. Grassberger and J. Procaccia. Characterization of strange attractors. Phys. Rev. Lett., 50:346–349, 1983. doi: 10.1103/PhysRevLett.50.346.
- [84] W. Grzesik and S. Brol. Wavelet and fractal approach to surface roughness characterization after finish turning of different workpiece materials. J. Materials Proc. Technol., 209:2522–2531, 2009. doi: 10.1016/j.jmatprotec.2008.06.009.
- [85] S. Günay. Source of the multifractality in exchange markets: Multifractal detrended fluctuations analysis. J. Bus. Econ. Res., 12:371–384, 2014. doi: 10.19030/jber.v12i4.8866.
- [86] I. Guttman and S. S. Wilks. Introductory engineering statistics. Wiley, New York, 1965.

- [87] I. Guttman, S. S. Wilks, and J. S. Hunter. Introductory engineering statistics. Wiley, New York, 1971.
- [88] S. Hadiyoso, I. Wijayanto, and A. Humairani. Signal dynamics analysis for epileptic seizure classification on eeg signals. Trait. Signal, 38:73–78, Feb 28 2021. doi: 10.18280/ts.380107.
- [89] S. Hadiyoso, I. Wijayanto, and I. Humairani. Entropy and fractal analysis of EEG signals for early detection of Alzheimer’s dementia. Traitement du Signal, 40:1673–1679, 2023r. doi: 10.18280/ts.400435.
- [90] L. J. Hadjileontiadis. Wavelet-based enhancement of lung and bowel sounds using fractal dimension thresholding-part i: methodology. IEEE Trans. Biomed. Engin., 52(6):1143–1148, 2005. doi: 10.1109/TBME.2005.846706.
- [91] H. Haken. Analogy between higher instabilities in fluids and lasers. Physics Lett. A, 53:77–78, 1975.
- [92] B. P. Harne. Higuchi fractal dimension analysis of eeg signal before and after om chanting to observe overall effect on brain. Int. J. Elect. Comp. Engin. (IJECE), 4:585–592, Agust 2014. URL <https://api.semanticscholar.org/CorpusID:121998800>.
- [93] F. J. Harris. On the use of windows for harmonic analysis with the discrete Fourier transform. Proc. IEEE, 66:51–83, 1978.
- [94] H. H. Hastings and G. Sugihara. Fractals. A User's Guide for the Natural Sciences. Oxford University Press, Oxford, 1993.
- [95] F. Hausdorff. Dimension und äußeres maß. Mathem. Ann., 79:157–179, 1918.
- [96] W. Heisenberg. Über den anschaulichen inhalt der quantentheoretischen kinematik und mechanik. Zeit. Physik, 43:172–198, 1927. doi: 10.1007/BF01397280.
- [97] N. Hemati. Strange attractors in brushless DC motors. IEEE Trans. Circ. Syst. I: Fundam. Theo. Appl., 41:40–45, 1994.
- [98] T. Higuchi. Approach to an irregular time series on the basis of the fractal theor. Physica D: Nonlin. Phen., 31:277–283, 1988. doi: 10.1016/0167-2789(88)90081-4.

- [99] T. Higuchi. Relationship between the fractal dimension and the power law index for a time series: A numerical investigation. Physica D: Nonlin. Phenom., 46:254–264, 1990. doi: 10.1016/0167-2789(90)90039-R.
- [100] M. Hollander and D. A. Wolfe. Nonparametric statistical procedures. Wiley, New York, 1st edition, 1973.
- [101] P. Hopkins, R. Sneyd, N. Outram, K. Rosén, and E. Ifeachor. Suitability of fractal dimension analysis of foetal heart rate as an indicator for asphyxia. In Proceedings of the International Conference on Computational Intelligence in Medicine and Healthcare (CIMED2005), Lisbon, Portugal, volume 2, pages 480–485, 2005.
- [102] P. Hopkins, N. Outram, N. Löfgren, E. C. Ifeachor, and K. G. Rosén. A comparative study of fetal heart rate variability analysis techniques. In 2006 International Conference of the IEEE Engineering in Medicine and Biology Society, pages 1784–1787. IEEE Engineering in Medicine and Biology Society, IEEE, 30 August 2006 – 03 September 2006.
- [103] S. Hossenfelder. Chaos: The real problem with quantum mechanics. YouTube, May 28 2022. URL <https://www.youtube.com/watch?v=LJzKLTavk-w&t=3s>.
- [104] S. Hossenfelder. Chaos: The real problem with quantum mechanics. YouTube, Dec 16 2023. URL <https://www.youtube.com/watch?v=KPUZiWMNeg>.
- [105] S. Hossenfelder. Is science dying? YouTube, Nov 18 2023 2023. URL <https://www.youtube.com/watch?v=KW4yBSV4U38>.
- [106] J. L. Hudson and J. C. Mankin. Chaos in the Belousov–Zhabotinskii reaction. J. Chem. Phys., 74:6171–6177, 1981. doi: 10.1063/1.441007.
- [107] H. E. Hurst. Long-term storage capacity of reservoirs. Trans.Am.Soc. Civil Eng., 116:770–808, 1951. doi: 10.1061/TACEAT.0006518.
- [108] H. E. Hurst. Methods of using long-term storage in reservoirs. Proc.Inst. Civil Eng., 5 Part 1:519–543, 1956. doi: 10.1680/iicep.1956.11503.
- [109] H. E. Hurst. The problem of long-term storage in reservoirs. Int. Assoc. Sci. Hydrol. Bull., 1:13–27, Ministry of Public Works , Egypt Published online: 04 Jan 2010. 1956. doi: 10.1080/02626665609493644.

- [110] H. E. Hurst. Methods of using long term storagf in reservoirs. Proc. Instit. Civil Engin., volume(5):519–543, Published Online: June 17, 2015 1956. doi: 10.1680/iicep.1956.11503.
- [111] T. Iokibe, S. Murata, M. Koyama, and T. Sugiura. A method for discrimination of arrhythmia by chaotic approach. In Proc. of the 1995 Int. Symp. on Nonlinear Theory and Its Applications (NOLTA), volume 95, pages 10–14, 1995. URL https://web.archive.org/web/20041106042600id_/http://www.riccx.com:80/j/paper/1995-4.pdf.
- [112] M. Jarraud, J. Goas, and C. Deyts. Prediction of an exceptional storm over France and southern England (15–16 October 1987). Weath Forecas., 4: 517–536, 1989.
- [113] G. Julia. Mémoire sur la permutabilité des fractions rationnelles. Annales Scientif. l’E.N.S. 3e, 39:131–215, 1922. URL <http://www.numdam.org/item/10.24033/asens.740.pdf>.
- [114] J. W. Kantelhardt. Fractal and multifractal time series. www.arxiv.org. Cornell University, Apr 4 y2008. URL <https://arxiv.org/pdf/0804.0747.pdf>.
- [115] L. P. Karakatsanis, G. P. Pavlos, and M. Xenakis. Statistical mechanics and its applications tsallis non-extensive statistics, intermittent turbulence, SOC and chaos in the solar plasma. Part two: Solar flares dynamics. Physica A, pages 3920–3944, Seph 15 2013. doi: 10.1016/j.physa.2013.05.010.
- [116] M. J. Katz. Fractals and the analysis of waveforms. Comput. Biol. Med., 18: 145–156, 1988. doi: 10.1016/0010-4825(88)90041-8.
- [117] W. Klonowski, E. Olejarczyk, R. Stepień, and W. Szelenberger. New methods of nonlinear and symbolic dynamics in sleep eeg-signal analysis. IFAC Proc. Vol., 36:241–244, 2003. doi: 10.1016/S1474-6670(17)33508-5.
- [118] E. Knobloch. Chaos in the segmented disc dynamo. Physics Lett. A, 82: 439–440, 1981.
- [119] C. G. Knot. Life and scientific work of Peter Guthrie Tait, supplementing the two volumes of Cambridge University Press. Cambridge University Press, Cambridge, UK, 1911. URL <http://tinyurl.com/4p4xmt9x>.
- [120] A. N. Kolmogorov. Three approaches to the quantitative definition of information. Prob. Inform.Transm., 1:1–7, 1964.

- [121] M. Kołodziej, A. Majkowski, W. Czop, P. Tarnowski, R. J. Rak, and D. Sawicki. Fall detection using a smartphone. In 21st International Conference on Computational Problems of Electrical Engineering (CPEE), pages 1–4, Pińczów, Poland, 2020. IEEE. doi: 10.1109/CPEE50798.2020.9238691.
- [122] E. Koscielny-Bunde, J. W. Kantelhardt, P. Braun, B. A. and S. Havlin. Long-term persistence and multifractality of river runoff records: Detrended fluctuation studies. www.arXiv.org, Cornell University, Jan 23 2004. URL <https://arxiv.org/pdf/physics/0305078.pdf>.
- [123] M. Krupiński, A. Wawrzaszek, W. Drzewiecki, M. Jenerowicz, and S. Aleksandrowicz. What can multifractal analysis tell us about hyperspectral imagery? Remote Sensing, 12:4077, 2020. doi: 10.3390/rs12244077.
- [124] J. Krzyszczak, P. Baranowski, M. Zubik, V. Kazandjiev, V. Georgieva, C. Sławiński, K. Siwek, J. Kozyra, and A. Nieróbca. Multifractal characterization and comparison of meteorological time series from two climatic zones. Theor. App. Climat., 137:1811–1824, 2018. doi: 10.1007/s00704-018-2705-0.
- [125] R. Kutner and F. świtała. Stochastic simulations of time series within weierstrass–mandelbrot walks. Quantitative Finance, 3:201–211, 2003. doi: 10.1088/1469-7688/3/3/306.
- [126] T. Lei. Similarity between the Mandelbrot set and Julia sets. Comm. Math. Physics, 134:587–617, 1990. doi: 10.1007/BF02098448.
- [127] L. Liehr and P. Massopust. On the mathematical validity of the higuchi method. www.arXiv.org, Cambridge University, Jun 25 2019. URL <https://arxiv.org/pdf/1906.10558.pdf>.
- [128] L. Liehr and P. Massopust. On the mathematical validity of the higuchi method. Physica D, 402:132265, 2019. doi: 10.1016/j.physd.2019.132265.
- [129] L. Liehr and P. Massopust. On the mathematical validity of the Higuchi method. Physica D: Nonlin. Phen., 402:32265, Jan 15 2020. doi: 10.1016/j.physd.2019.132265.
- [130] J. Z. Liu, Q. Yang, B. Yao, R. W. Brown, and G. H. Yue. Linear correlation between fractal dimension of eeg signal and handgrip force. Biol. Cybern., 93:131–140, 2005. doi: 10.1007/s00422-005-0561-3.
- [131] A. C. Lorenc, R. S. Bell, T. Davies, and C. J. Shutts. Numerical forecast studies of the October 1987 storm over southern England. Mereorol. Mag., 43:90–110, 1988. doi: 10.1002/j.1477-8696.1988.tb03885.x.

- [132] E. Lorenz. The predictability of a flow which possesses many scales of motion. Tellus, 21:289–307, 1969. doi: 10.1111/j.2153-3490.1969.tb00444.
- [133] E. N. Lorenz. Deterministic nonperiodic flow. J. Atm. Sci., 20:130–141, 1963. doi: 10.1175/1520-0469(1963)020<0130:DNF>2.0.CO;2.
- [134] A. M. J. M. Machorro-Lopez, J. P. Amezcuita-Sanchez, C. A. Perez-Ramirez, M. Valtierra-Rodriguez, and A. Dominguez-Gonzalez. Fractal dimension analysis for assessing the health condition of a truss structure using vibration signals. Fractals, 28:2050127, Jun 10 2020. doi: 10.1142/S0218348X20501273.
- [135] B. Mandelbrot. The variation of certain speculative prices. J. Business, 36: 394–419, 1963. doi: 10.1007/978-1-4757-2763-0_14.
- [136] B. B. Mandelbrot. The Beauty of Fractals, chapter Fractals and the rebirth of iteration theory, pages 151–160. Springer–Verlag, Santa Cruz, CA 95064, USA, 1966.
- [137] B. B. Mandelbrot. How long is the coast of Britain? Statistical self-similarity and fractional dimension. Science, 156:636–638, 1967. doi: 10.1126/science.156.3775.636.
- [138] B. B. Mandelbrot. Fractal aspects of the iteration of for complex. Ann. N.Y. Acad. Sci., 357:249–259, 1980. doi: 10.1111/j.1749-6632.1980.tb29690.x.
- [139] B. B. Mandelbrot. The Fractal Geometry of Nature. W.H. Freeman and Co., New York, 1983.
- [140] B. B. Mandelbrot. Fractals and the rebirth of iteration theory. In H. Peitigen and P. H. Richter, editors, The beauty of fractals. Springer-Verlag, Berlin, 1986. doi: 10.1007/978-3-642-61717-1_12.
- [141] B. B. Mandelbrot. The Beauty of Fractals. Images of Complex Dynamical Systems. Springer-Verlag, Berlin, 1986.
- [142] B. B. Mandelbrot. Fractals and Scaling in Finance, chapter The variation of certain speculative prices, pages 371–418. Springer Science+Business Media, New York, NY, USA, 1997.
- [143] B. B. Mandelbrot. Gaussian self-affinity and fractals (selecta volume h), 2002.

- [144] B. B. Mandelbrot and A. Blumen. Fractal geometry: What is it, and what does it do? Proc. Royal Soc. A: Mathem. Phys. Engin. Sci., 22:L377–L383, 1989. doi: 10.1098/rspa.1989.0038.
- [145] B. B. Mandelbrot and T. Vicsek. Directed recursion models for fractal growth. J. Physics A: Mathematical and General, 22:L377–L383, 1989.
- [146] B. B. Mandelbrot and J. R. Wallis. Some long-run properties of geophysical records. Wat. Res. Research, 5:321–340, 1969. doi: 10.1029/WR005i002p00321.
- [147] D. Mayor, T. Steffert, A. Firth, H. Kandel, and D. Banks. Complexity and entropy in physiological signals (CEPS): Resonance breathing rate assessed using measures of fractal dimension, heart rate asymmetry and permutation entropy. Entropy, page 301, 2023. doi: 10.3390/e25020301.
- [148] C. McGinty. The McGinty Equation: Unifying Quantum Field Theory and Fractal Theory to Under Skywise Marketing Solutions LLC, Amazon Kindle edition edition, Mar 23 2023. 94 pages.
- [149] C. McGinty. The McGinty Equation and its Modified Forms: Towards a Unified Framework for Quantum Physics, Field Theory, and Gravity. Int. J. Theo, Comput. Phys., 4:1–13, 2023. doi: 10.47485/2767-3901.1034. URL <http://tinyurl.com/sz7fmxjm>.
- [150] M. I. Meltzer. The potential use of fractals in epidemiology. Prev. Vet. Med., 11:255–260, 1991. doi: 10.1016/s0167-5877(05)80011-x.
- [151] S. P. Meyn and R. L. Tweedy. Markov chains and stochastic stability. Springer–Verlag, London, UK, 1993.
- [152] J. W. Milnor. Attractor. Scholarpedia, the peer-reviewed open-access encyclopedia, Nov 3 2006. URL <http://scholarpedia.org/article/Attractor>.
- [153] M. C. Montero, M. del Campo, M. Bono, M. V. Simon, J. Guerrero, and N. Lagos. Neosaxitoxin inhibits the expression of inflammation markers of the M1 phenotype in macrophages. Mar. Drugs, 18:1–17, May 27 2020. doi: 10.3390/md18060283.
- [154] J. M. Muroki. Dynamic vehicle routing model using geometric brownian motion. Master’s thesis, Faculty of Information Technology, Strathmore University Library, Nairobi, Kenya, Jun 2019. URL <https://>

[//su-plus.strathmore.edu/server/api/core/bitstreams/
b7a935a5-1d9a-4178-9c1b-4637f3ce8501/content](https://su-plus.strathmore.edu/server/api/core/bitstreams/b7a935a5-1d9a-4178-9c1b-4637f3ce8501/content).

- [155] V. Nepiklonov, E. Spiridonova, and M. Maksimova. Fractal analysis of global model dynamics earth's gravitational fieldle. Geodes. Photo Sys., 64:380–390, 2020. doi: 10.30533/0536-101X-2020-64-4-380-390.
- [156] S. Newhouse, D. Ruelle, and F. Takens. Occurrence of strange AxiomA attractors near quasi periodic flows $ont^m, m \geq 3$. Commun.Math. Phys., 64: 35–40, Oct 31 1978. doi: 10.1007/BF01940759.
- [157] G. Nicolis and I. Prigoyine. Exploring Complexity. An Introduction. W.H. Freeman and Co., New York, 1989.
- [158] A. W. Oppenheim and R. W. Schaffer. Digital Signal Processing. Prentice-Hall Inc., Egelwood Cliffs, NJ, 1975.
- [159] P. J. Ossenbruggen and E. M. Laflamme. Explaining freeway breakdown with geometric brownian motion mode. J. Transp. Engin., Part A: Systems, 145:04019037, 2019. doi: 10.1061/JTEPBS.0000255.
- [160] P. E. O'Connell, D. Koutsoyiannis, H. F. Lins, Y. Markonis, A. Montanari, and T. Cohn. The scientific legacy of Harold Edwin Hurst (1880–1978). Hydrol. Sci. J., 61:1571–1590, 2016. doi: 10.1080/02626667.2015.1125998.
- [161] T. Palmer. The butterfly effect - What does it really signify? YouTube, Oxford Mathematics, Retrieved: October 23 2022. URL <https://www.youtube.com/watch?v=vkQEqXAz44I>.
- [162] Y. Pan, P. M. Silveira, T. L. Baldwin, and P. F. Ribeiro. A fault location approach for high-impedance grounded dc shipboard power distribution systems. In Conversion and Delivery of Electrical Energy in the 21st Century, pages 1–6, Pittsburgh, PA, USA, 20-24 July 2008. IEEE, IEEE. doi: 10.1109/PES.2008.4596844.
- [163] G. Pavlos, L. Karakatsanis, and M. Xenakis. Tsallis non-extensive statistics, intermittent turbulence, SOC and chaos in the solar plasma, Part one: Sunspot dynamics. Physica A, 391:6287–6319, Aug 4 2012. doi: 10.1016/j.physa.2012.07.066.
- [164] J. L. Pe. Fractal dimension, primes, and the persistence of memory. Adv. Comp. Syst., 6:241–249, 2003. doi: 10.1142/S0219525903000864Citedby:0.

- [165] S. M. Pincus. Approximate entropy as a measure of system complexity. Proc. Nati. Acad. Sci. USA, 88:2297–2301, 1991.
- [166] S. M. Pincus. Assessing serial irregularity and its implications for health. Ann. NY Acad. Sci., 954:245–267, 2001.
- [167] S. M. Pincus. Assessing serial irregularity and its implications for health. Ann. New York Acad. Sci., 954:245–267, 2006. doi: 10.1111/j.1749-6632.2001.tb02755.x.
- [168] S. M. Pincus, I. M. Gladstone, and R. A. Ehrenkranz. A regularity statistics for medical data analysis. J. Clin. Monit., 7:335–345, 1991. doi: 10.1007/BF01619355.
- [169] J. Pitman. Probability. Springer Texts in Statistics. Springer Verlag, New York, 1st edition, 1993.
- [170] D. Poland. Cooperative catalysis and chemical chaos: A chemical model for the Lorenz equations. Physica D, 65:86–99, 1993.
- [171] N. Pradhan and N. D. Dutt. Use of running fractal dimension for the analysis of changing patterns in electroencephalograms. Comp. Biol. Med., 23:381–388, 1993. doi: 10.1016/0010-4825(93)90135-n.
- [172] W. H. Press, S. A. Teukolsky, W. T. Vetterling, and B. P. Flannery. Numerical Recipes. The Art of Scientific Computing. Cambridge University Press, Cambridge, UK, 3rd edition, 2007.
- [173] P. Purkait and S. Chakravorti. Impulse fault classification in transformers by fractal analysis. IEEE Trans. Dielect. Elect. Insul., 10:109–116, Feb 2003. doi: 10.1109/TDEI.2003.1176571\.
- [174] A. V. P.-S. qnd M. ValtietaA-Rodriguez, C. A. Perez-Ramirez, J. J. De-Santiago-Perez, and J. P. Amezoutia-Sanchez. Epileptic seizure prediction using wavelet transform, fractal dimension, support vector machine, and EEG signals. Fractals, page Online, Jul 28 2022. doi: 10.1142/S0218348X22501547.
- [175] D. R. The Hausdorff dimension of the nondifferentiability set of the Cantor function is $[\ln(2)/\ln(3)]^2$. Proc. Am. Math. Soc., 119:105–108, 1993. doi: 10.1090/S0002-9939-1993-1143222-3.

- [176] B. Raghavendra and D. N. Dutt. A note on fractal dimensions of biomedical waveforms. Comp. Biol. Med., 39:1006–1012, 2009. doi: 10.1016/j.combiomed.2009.08.001.
- [177] I. Ramirez-Vazquez and J. R. J. E. Salgado-Talavera. Fractal analysis of nano-reinforced silicone rubber insulators evaluated on a tracking wheel. EEE Electr. Insul. Mag., 30:21–27, Jun 26 2014. doi: 10.1109/MEI.2014.6843764.
- [178] H.-G. P. P. H. Richter, editor. The Beauty of Fractals. Images of Complex Dynamical Systems. Springer-Verlag, Berlin, 1986.
- [179] A. J. Rodríguez-Hernández and C. Sevcik. Hidden chaos factors inducing random walks which reduce hospital operative efficiency. PLoS One, page Online: e0262815, Jan 27 2022. doi: 10.1371/journal.pone.0262815.
- [180] J. Samuel, L. Combinido, and M. T. Lim. Crowding effects in vehicular traffic. PLOS One, 7:e48151, Nov 5 2012. doi: 10.1371/journal.pone.0048151.
- [181] M. Sánchez, J. E. Trinidad, J. García, and F. M. The effect of the underlying distribution in hurst exponent estimation. PLoS ONE, 10:e0127824, 2015. doi: 10.1371/journal.pone.0127824.
- [182] M. A. Savageau. Michaelis-Menten mechanism reconsidered: implications of fractal kinetics. J. Theor. Biol., 176:115–124, 1995. doi: 10.1006/jtbi.1995.0181.
- [183] C. Sevcik. Fractal analysis of Pi normality. www.arXiv.org, Cornell University. URL <https://arxiv.org/pdf/1608.00430.pdf>.
- [184] C. Sevcik. A procedure to estimate the fractal dimension of waveforms. Complexity Internat., 5:1–19 (Original unavailable please discharge from <https://arxiv.org/pdf/1003.5266.pdf>, 1998.
- [185] C. Sevcik. A procedure to estimate the fractal dimension of waveforms. www.archiv.org, Cornell University, Mar 27 2010. URL <https://arxiv.org/pdf/1003.5266.pdf>.
- [186] C. Sevcik. Fractal analysis of Pi normality. Exper. Mathem., 27:331–343, 2017. doi: 10.1080/10586458.2017.1279092.
- [187] E. Shamsi, M. A. Ahmadi-Pajouh, and T. S. Ala. Higuchi fractal dimension: An efficient approach to detection of brain entrainment to theta binaural beats. Biomed. Sig. Proc. Cont., 68:102580, month 2021. doi: 10.1016/j.bspc.2021.102580.

- [188] C. E. Shannon. A mathematical theory of communication. Bell Sys. Tech. J., 27:379–423, 1948.
- [189] C. E. Shannon. Communication in the presence of noise. Proc. Inst. Radio Engin., 37:10—21, 1949.
- [190] N. Sharma and J. K. Ghosh. Sevcik’s fractal based dimensionality reduction of hyper-spectral remote sensing data. Internat. J. Comp. Sci. Tech, 4:52–55, 2013. URL https://www.researchgate.net/publication/257760116_Sevcik's_Fractal_Based_Dimensionality_Reduction_of_Hyper-Spectral_Remote_Sensing_Data_1.
- [191] C.-T. Shi. Signal pattern recognition based on fractal features and machine learning. Appl. Sci., 8:1327, Aug 8 2018. doi: 10.3390/app8081327.
- [192] X. Shi, M. Ye, S. Finsterle, and J. Wu. Comparing nonlinear regression and Markov chain Monte Carlo methods for assessment of prediction uncertainty in vadose zone modeling. Vadose Zone J., 11(4):vzj2011–0147, 2012. doi: 10.2136/vzj2011.0147.
- [193] W. Sierpinski. Elementary Theory of Numbers. North-Holland Mathematical Library. North Holland—PWN- Polish Scientific Publishers, Amsterdam – Warszawa, 2nd edition, 1988.
- [194] L. Silva, M. Vermelho, M. Lyra, and G. Viswanathan. Multifractal detrended fluctuation analysis of analog random multiplicative processes. Chaos Sol. Fract., 41:2806–2811, 2009. doi: 10.1016/j.chaos.2008.10.027.
- [195] Y. Sinai. On the notion of entropy of a dynamical system. Doklady Russ. Acad. Sci., 124:768–771, 1959.
- [196] S. W. Smith. The Scientist and Engineer’s Guide to Digital Signal Processing. California Technical Publishing, San Diego, CA, 1997.
- [197] L. R. Snyder, J. W. Dolan, and J. R. Gant. Gradient elution in high-performance liquid chromatography: I. Theoretical basis for reversed-phase system. J. Chromatogr., 165:3–30, 1979.
- [198] S. Spacic, S. Kecic, A. Kalauzi, and J. Saponjic. Different anesthesia in rat induces distinct inter-structure brain dynamic detected by Higuchi fractal dimension. Fractals, 19:113–123, 2011. doi: 10.1142/S0218348X1100521X.

- [199] S. Spasica, A. Kalauzi, S. Kesic, M. Obradovic, and J. Saponjic. Surrogate data modeling the relationship between high frequency amplitudes and Higuchi fractal dimension of EEG signals in anesthetized rats. J. Theoret. Biol., 289:160–166, Nov 21 2011. doi: 10.1016/j.jtbi.2011.08.037.
- [200] J. Sutcliffe, A. G. Awadallah, E. Brown, and K. Hamed. Harold Edwin Hurst: the Nile and Egypt, past and future. Hydr. Sci. – J. Sciences Hydrauliq., 61: 1557–1570, 2016. doi: 10.1080/02626667.2015.1019508.
- [201] J. V. Sutcliffe. Obituary. Hydrol. Sci. Bull., 24:539–541, 1979. doi: 10.1080/02626667909491892. URL <https://www.tandfonline.com/doi/abs/10.1080/02626667909491892>.
- [202] J. V. Sutcliffe and Y. P. Parks. The Hydrology of the Nile. International Association of Hydrological Sciences, 1999. ISBN 5. URL <http://www.hydrosciences.fr/SIEREM/Bibliotheque/biblio/hydrology%20of%20the%20Nile.pdf>.
- [203] L. Szilárd. Über die entropieverminderung in einem thermodynamischen System bei Eingriffen intelligenter Wesen. Zeitsch. Physik, 53(11):840–856, 1929. doi: 10.1007/BF01341281. URL <https://fab.cba.mit.edu/classes/862.19/notes/computation/Szilard-1929.pdf>.
- [204] L. Telesca and V. Lapenna. Measuring multifractality in seismic sequences. Tectonophysics, 423:115–123, 2006. doi: 10.1016/j.tecto.2006.03.023.
- [205] L. Telesca, V. Lapenna, and M. Macchiato. Multifractal fluctuations in seismic interspike series. Physica A: Stat. Mechan. Appl., 354:629–640, 2005. doi: 10.1016/j.physa.2005.02.053.
- [206] D. H. Terman and E. M. Izhikevich. State space. Scholarpedia, the peer-reviewed open-access encyclopedia, Feb 29 2008. URL http://www.scholarpedia.org/article/State_space.
- [207] J. Theiler. Estimating fractal dimension. J. Opt. Soc. Am. A, pages 1055–1073, 1990. doi: 10.1364/JOSAA.7.001055.
- [208] K. Thomas and H. Dia. Development and evaluation of fractal dimension models for freeway incident detection. Road Transp. Res., 13:2–20, 2004.
- [209] A. M. Turing. The chemical basis of morphogenesis. Philos. Trans. Royal Soc. London, 237 B:37–72, 1952. doi: 10.1098/rstb.1952.0012. URL <https://www.dna.caltech.edu/courses/cs191/paperscs191/turing.pdf>.

- [210] M. Valtierra-Rodriguez. Fractal dimension and data mining for detection of short-circuited turns in transformers from vibration signals. Meas. Sci. Tech., 31(2):025902, Nov 2019. doi: 10.1088/1361-6501/ab48ac.
- [211] H. von Koch. Sur une courbe continue sans tangente, obtenue par une construction géométrique élémentaire. Archiv für Matemat., Astron. och Fys., 1:681–702, 1904.
- [212] D. F. Vysochanskiï and Y. I. Petunin. Justification of the 3σ rule for unimodal distributions. Theor. Probab. Math. Stat., 21:25–36, 1980.
- [213] D. F. Vysochansky and Y. I. Petunin. Justification of the 3σ rule for unimodal distributions. Theor. Probab. Math. Stat., 21:23–35, 1979.
- [214] D. F. Vysochansky and Y. I. Petunin. A remark on the paper ‘Justification of the 3σ rule for unimodal distributions’. Theor. Probab. Math. Stat., 27: 27–29, 1983.
- [215] C. Walck. Hand-book on statistical distributions for experimentalists. Technical Report SUF–PFY/96–01, Particle Physics Group, Fysikum, University of Stockholm, Stockholm, Last modification 10 September 2007. 1996. URL <https://www.stat.rice.edu/~dobelman/textfiles/DistributionsHandbook.pdf>.
- [216] P. D. Welch. The use of fast Fourier transform for the estimation of power spectra: A method based on time averaging over short, modified periodograms. IEEE Trans. Audio Electr., AU-15:70–73, 1967. doi: 10.1109/TAU.1967.1161901.
- [217] S. S. Wilks. Mathematical Statistics. Wiley, New York, 1962.
- [218] W.Klonowski, E.Olejarczyk, and R.Stepien. Sleep-eeg analysis using higuchi’s fractal dimension. In 2005 International Symposium on Nonlinear Theory and its Applications (NOLTA2005), Bruges, Belgium, Oct 18-21 2005. NOLTA’Bruges. URL https://www.researchgate.net/publication/267548779_Sleep-EEG_Analysis_Using_Higuchi%27s_Fractal_Dimension.
- [219] S. Wolfram. The Mathematica[®] Book. Wolfram Media, Champagn, IL, 5th edition, 2003.
- [220] F. Xu and H. Ding. A new kinetic model for heterogeneous (or spatially confined) enzymatic catalysis: Contributions from the fractal and jamming

- (overcrowding) effects. App. Catal. A: General, 317:70–81, 2007. doi: 10.1016/j.apcata.2006.10.014.
- [221] R. Xue, J. Liu, and H. Tang. Two-dimensional jamming recognition algorithm based on the Sevcik fractal dimension and energy concentration property for UAV frequency hopping systems. Information, 11:520, 2020. doi: 10.3390/info11110520.
- [222] Y. Yuan and X. Zhuang. Multifractal description of stock price index fluctuation using a quadratic function fitting. Physica A: Stat. Mech. Appl., 387: 511–518, 2008. doi: 10.1016/j.physa.2009.02.026.
- [223] Y. Yuan, X. Zhuang, and X. Jin. Measuring multifractality of stock price fluctuation using multifractal detrended fluctuation analysis. Physica A: Stat. Mech. Appl., 388:2189–2197, 2009. doi: 10.1016/j.physa.2009.02.026.
- [224] A. Zhabotinsky. Belousov-zhabotinsky reaction. Scholarpedia, 2(9):1435, 2007. doi: 10.4249/scholarpedia.1435.
- [225] W. H. Zurek. Decoherence, einselection, and the quantum origins of the classical. www-arXiv.org, Cornell University, Jun 19 2003. URL <https://arxiv.org/pdf/quant-ph/0105127.pdf>.